The Gag Protein PEG10 Binds to RNA and Regulates Trophoblast Stem Cell Lineage Specification.

Mona Abed[a], Erik Verschueren[b], Hanna Budayeva[b], Peter Liu[b], Donald S. Kirkpatrick[b], Rohit Reja[c], Sarah K. Kummerfeld[c,g], Joshua D. Webster[d], Sarah Gierke[d], Mike Reichelt[d], Keith R. Anderson[e], Robert J Newman[e], Merone Roose-Girma[e], Zora Modrusan[e], Hazal Pektas[f], Emin Maltepe[f], Kim Newton[a], Vishva M. Dixit[a]

Departments of Physiological Chemistry[a], Protein Chemistry[b], Bioinformatics and Computational Biology[c], Pathology[d], and Molecular Biology[e], Genentech, 1 DNA Way, South San Francisco, CA 94080, USA. [f]The Center for Reproductive Sciences, Division of Neonatology, University of California, San Francisco, CA, 94143.

[g]Current address: Kinghorn Centre for Clinical Genomics, Garvin Institute of Medical Research, 370 Victoria Street, Darlinghurst, NSW 2010, Australia.

Correspondence to VMD (dixit@gene.com; +1-650-225-1312)

Short Title: The role of PEG10 in trophoblast stem cells.

ABSTRACT

Peg10 (paternally expressed gene 10) is an imprinted gene that is essential for placental development. It is thought to derive from a Ty3-gyspy LTR (long terminal repeat) retrotransposon and retains Gag and Pol-like domains. Here we show that the Gag domain of PEG10 can promote vesicle budding similar to the HIV p24 Gag protein. Expressed in a subset of mouse endocrine organs in addition to the placenta, PEG10 was identified as a substrate of the deubiquitinating enzyme USP9X. Consistent with PEG10 having a critical role in placental development, PEG10-deficient trophoblast stem cells (TSCs) exhibited impaired differentiation into placental lineages. PEG10 expressed in wild-type, differentiating TSCs was bound to many cellular RNAs including *Hbegf* (Heparin-binding EGF-like growth factor), which is known to play an important role in placentation. Expression of *Hbegf* was reduced in PEG10-deficient TSCs suggesting that PEG10 might bind to and stabilize RNAs that are critical for normal placental development.

INTRODUCTION

Transposable elements (TEs) are one of the biggest threats to the integrity of prokaryotic and eukaryotic genomes because their insertion into coding or regulatory regions could disrupt essential genes (1-3). Therefore, TEs are often inactivated through mutagenesis (4) or silenced through methylation (5). Some TEs, however, have been repurposed during evolution for the benefit of the host in a process termed domestication (6), and have important roles in development and immunity (7-10).

Peg10 is a domesticated TE that is expressed in eutherian mammals (8, 11). It has lost the ability to transpose, but retains the retroviral characteristic of frameshifting (FS) that allows the

translation of two overlapping reading frames from the same transcript (12). Thus, *Peg10* encodes PEG10-RF1 corresponding to the structural Gag-like protein, as well as PEG10-RF1/2 representing a fusion of the Gag and Pol domains (12). *Peg10*-deficient mouse embryos are not viable because *Peg10* is required for formation of the labyrinth and spongiotrophoblast layers of the placenta (13). Precisely how the PEG10 proteins exert this function is unclear. Whether *PEG10*, which is also expressed in the human testis and ovary (14), has functions outside of the placenta is likewise unclear. Interestingly, *PEG10* is aberrantly expressed in some human tumors including hepatocellular carcinomas (14) and neuroendocrine prostate cancers (15).

Here we study the role of PEG10 in mouse embryonic stem cells (ESCs) and trophoblast stem cells (TSCs) after identifying it as a substrate of the deubiquitinating enzyme USP9X. Expressed in several stem cell populations (16-18) as well as in differentiated cell types, USP9X is essential for mouse development (19). Diverse substrates of USP9X have been reported, including the pro-survival protein MCL-1 (20), the kinase ZAP70 (21), and the E3 ubiquitin ligases SMURF1 (22) and FBW7 (23), but it is unclear if these are critical substrates of USP9X in ESCs and TSCs.

MATERIALS AND METHODS

ESCs and TSCs.

The Genentech institutional animal care and use committee approved all mouse protocols. *Usp9x*$^{fl/y}$ *Rosa26*$^{+/CreERT2}$ ESCs were derived from blastocysts after crossing *Rosa26*^{CreERT2} (24) and *Usp9x*^{fl} (19) mice. Blastocysts were cultured on irradiated mouse embryo fibroblasts (PMEF-N, Millipore Sigma) in ESGRO-2i medium (Millipore Sigma SF016-100) for 13 days to produce ESCs. The cells were subsequently maintained on PMEF-N cells in KNOCK-OUT

66 medium (Invitrogen) supplemented with 1000 U LIF (EMD Millipore), 15% fetal bovine serum
67 (GE Health), 1× non-essential amino acids (Gibco), 2 mM L-glutamine (Gibco), and 50 µM 2-
68 mercaptoethanol (EMD Millipore). A 3xFLAG sequence was inserted after the initiator ATG in
69 *Peg10* by homologous recombination. *Usp9x*$^{3xf/y}$ and *Usp9x*$^{C1566A/y}$ ESCs were generated by
70 Taconic (Germany) using C57BL/6 NTac ESCs. In brief, a 3xFLAG sequence was inserted after
71 the initiator ATG in *Usp9x* exon 2 (*Usp9x*$^{3xf/y}$ ESCs) or the TGT codon encoding Cys1566 in
72 *Usp9x* exon 31 was changed to GCC (*Usp9x*$^{C1566A/y}$ ESCs).
73
74 TSCs were prepared as described (25) and cultured on plates pre-treated with CellStart substrate
75 (A1014201, Thermo Fisher) for 2 h at 37℃. TSC culture medium was RPMI1670 containing 20%
76 FBS, 1 mM sodium pyruvate, 2 mM L-glutamine, 50 µg/mL penicillin/streptomycin, 100 µM 2-
77 mercaptoethanol, 0.1 mM FGF4 (F2278, Sigma), and 1 µg/mL Heparin (H3149, Sigma). For TSC
78 differentiation, cells were split to a 30% density without CellStart, FGF4 or heparin, and cultured
79 at 20% or 2% oxygen for 5-10 days while changing media every other day. For TSC transfection,
80 cells were plated at 20% density on CellStart with FGF4 and Heparin, and then transfected the day
81 after using Effectene transfection reagent (301425, Qiagen).
82
83 PEG10-deficient ESCs and TSCs were generated using a two cut CRISPR strategy. Cells were
84 co-transfected with pRK-Cas9 (38), *Peg10* 5' sgRNA (CTC TCA CCG CAG CCA TGG C) and
85 3' sgRNA (GCA TCA TCC TGC AGT GCT G). sgRNAs were expressed from U6 promoters on
86 individual plasmids.
87

Antibodies.

Antibodies recognized GAPDH (G9545, Sigma), PEG10 (Genentech monoclonal antibodies were raised against mouse PEG10 residues A2-V377; rat clone 17D4D6C2 was used for western blotting and immunofluorescence, mouse clone 36E2B2B4 was used for immunoprecipitations, and rat clone 5H7B1E3 was used for immuno-gold electron microscopy), USP9X (5679, Genentech), Syntaxin 8 (12206-1-AP, Proteintech), VTI1B (ab184170 Abcam), ABCD3 (ab3421, Abcam), ERK (9102, Cell Signaling), phospho-ERK (9101, Cell Signaling), MEK (4694, Cell Signaling), phospho-MEK (9154, Cell Signaling), p70 S6 Kinase (2708, Cell Signaling), phospho-p70 S6 Kinase (9234, Cell Signaling), Akt (4691, Cell Signaling), phospho-Akt (4060, Cell Signaling), FLAG (A8592, Sigma), HIV1 p24 (ab9071 Abcam), Sall4 (sc-101147, Santa Cruz Biotechnology), and TSG101 (GTX70255, GeneTex).

Immunoprecipitation and fractionation.

Cells were dounced in 10 mM Tris pH 7.4, 7.5 mM KCl, 1.5 mM $MgCl_2$, 5 mM 2-mercaptoethanol, plus complete protease inhibitor and PhosSTOP phosphatase inhibitor cocktails (Roche). Insoluble material was removed by centrifugation. The soluble material was adjusted to 20 mM Tris pH 7.4, 135 mM KCl, 1.5 mM $MgCl_2$, 2 mM EDTA, 2% Triton, and 20% glycerol before immunoprecipitation of PEG10 or USP9X. Immunoprecipitations with anti-FLAG M2 beads (Sigma) were eluted with FLAG or 3xFLAG peptide as appropriate. Cell lysates were fractionated with NE-PER Nuclear and Cytoplasmic Extraction Reagent (78833, Thermo Scientific).

Affinity purification mass spectrometry experiments.

Protein bands were excised into 10 gel pieces from top to bottom for each pulldown. The pieces were further de-stained in 50 mM NH_4HCO_3/50% acetonitrile (ACN), dehydrated in 100% ACN, and re-hydrated in 10 ng/µL trypsin on ice for 20 min. After removing the excess trypsin solution, digestion was performed at 37˚C overnight in 25 mM NH_4HCO_3. Peptides were extracted in 1% formic acid (FA)/50% ACN, then 100% ACN, and dried in a SpeedVac. After reconstitution in solvent A (2% ACN/0.1% FA), peptides underwent reverse phase chromatography on a NanoAcquity UPLC system (Waters). Peptides were loaded onto a Symmetry® C18 column (1.7 mm BEH-130, 0.1 x 100 mm) with a flow rate of 1 µL/min and a gradient of 2% to 25% Solvent B (0.1% FA/2% water/ACN). Peptides were eluted directly into an Advance CaptiveSpray ionization source (Michrom BioResources/Bruker) with a spray voltage of 1.2 kV, and analyzed using an LTQ Orbitrap Elite mass spectrometer (ThermoFisher). Precursor ions were analyzed in the FTMS at 60,000 resolution; MS/MS data was acquired in the LTQ with the instrument operated in data-dependent mode, whereby the top 15 most abundant ions were subjected to fragmentation.

MS/MS spectra were searched using the Mascot algorithm (Matrix Sciences) against a concatenated target-decoy database comprised of the UniProt Mus musculus protein sequences (downloaded June 2016), known contaminants, and the reversed versions of each sequence. A 50 ppm precursor ion mass tolerance and 0.8 Da fragment ion tolerant were selected with tryptic specificity up to 3 missed cleavages. Fixed modifications were allowed for carbamidomethylated cysteine residues (+57.0215 Da) and variable modifications were permitted for methionine oxidation (+15.9949 Da). Peptide assignments were first filtered to a 1% False Discovery Rate (FDR) at the peptide level and subsequently to a 2% FDR at the protein level. Peptide Spectral

Matches (PSMs) per protein were summed across all fractions from the GelC-MS experiment for each IP separately. SAINTExpress-spc v.3.6.1 (26) was run with default settings, comparing the sum of PSMs for all identified proteins enriched with the IP antibody to their negative controls, for each AP-MS experiment separately. Interactions with a SAINT score > 0.9, Bayesian False Discovery Rate (BFDR) < 0.05, and average sum PSM count > 10 were marked.

Ubiquitin substrate profiling.

ESC lysate (40 mg) was prepared under denaturing conditions, reduced and alkylated, diluted 4-fold, and then subjected to overnight trypsin digestion. Peptides were acidified with trifluoroacetic acid (TFA), desalted by solid-phase extraction, and lyophilized for 48 h. Dry peptides were resuspended in 1x IAP buffer (Cell Signaling Technologies), clarified by centrifugation, then incubated with anti-KGG coupled resin (Cell Signaling Technologies) for 2 h at 4°C. Beads were washed twice with IAP buffer, four times with water, and eluted twice using 0.15% TFA. Peptide eluates were desalted using STAGE-Tips and analyzed using an Orbitrap-Elite mass spectrometer as described previously (27). Peptide spectral matching was performed using semi-tryptic specificity and ±25 ppm mass precursor tolerance using Mascot (Matrix Science). A target-decoy database comprised mouse proteins (UniProt ver. 2011_12) and common contaminants. Oxidized methionine (+15.9949) and K-GG (+114.0429) were considered as variable modifications, carbamidomethyl cysteine (+57.0214) as a fixed modification, and two missed cleavage events were permitted. Peptide spectral matches were filtered serially using linear discriminant analysis to 5% and 2% FDR at the peptide and protein levels, respectively. Label–free peak areas were determined for confidently identified peptides using the XQuant algorithm and consolidated at the protein level using linear mixed effects modeling as described previously (28).

155

156 **Global proteome and phosphoproteome analysis.**

157 Cells were lysed in 20 mM HEPES pH 8.0, 9 M urea, and phosphatase inhibitor cocktail (Roche).
158 Lysates were sonicated on a microtip and insoluble material was removed by centrifugation.
159 Approximately 30 mg of total protein per condition was reduced and alkylated in 5 mM DTT and
160 15 mM iodoacetamide, respectively. Protein mixtures were diluted 4-fold in 20 mM HEPES, pH
161 8.0 and sequentially digested with LysC (1:50, enzyme:protein, Wako) and trypsin (1:100,
162 enzyme:protein, Thermo Fisher Scientific). Peptide mixtures were purified on SepPak columns
163 (Waters) and lyophilized to dryness. An aliquot of the digested peptides from each condition was
164 processed for global proteome profiling. Briefly, 200 µg of total peptides per condition were
165 labeled with tandem mass tag (TMT10plex and TMT11, Thermo Fisher Scientific). After >98%
166 TMT incorporation rate was confirmed, samples were combined and fractionated by high pH
167 Reverse Phase LC (Agilent Technologies) into 24 fractions for analysis as described previously
168 (29).

169

170 From the majority of the sample, phosphopeptides were enriched using TiO_2 titansphere resin (GL
171 Sciences). Peptides were reconstituted in 50% ACN and 2 M lactic acid buffer, and incubated at
172 1:5 peptide:titansphere ratio for 2 h at room temperature. The titansphere particles were washed
173 sequentially in 50% ACN/2M lactic acid, 50% ACN/0.1% TFA, and 25% ACN/0.1% TFA.
174 Phosphopeptides were eluted with 50 mM K_2HPO_4 pH 10 buffer and lyophilized. Enriched
175 peptides were labeled with TMT10plex and TMT11 reagents (Thermo Fisher Scientific). Samples
176 were combined and processed for phosphotyrosine (pY) enrichment using p100 PTMScan reagent

(Cell Signaling Technologies). The flow-through fraction (pST) was subject to high pH reverse phase fractionation into 24 fractions for analysis as described previously (29).

Liquid chromatography and tandem mass spectrometry.

TMT-labeled peptides for global proteome, KGG, pST and pY profiling were desalted on C18 stage tip, dried by vacuum centrifugation, and reconstituted in 2% ACN/0.1% FA for analysis. All samples were analyzed by liquid chromatography coupled to tandem mass spectrometry (LC-MS) on Dionex Ultimate 3000 RSLCnano system (Thermo Fisher Scientific) and Orbitrap Fusion Lumos Tribrid MS (Thermo Fisher Scientific). Peptide samples were resolved by 158 min linear gradient of 2% to 30% buffer B (98% ACN/0.1% FA) in buffer A (2% ACN/0.1% FA) on 100 µm ID PicoFrit column packed with 1.7 µm Acquity BEH (New Objective) at a flow rate of 450 nL/min. Total run length including injection, gradient, column washing and re-equilibraton was 180 min. Multi-Notch MS3-based TMT method was used for sample analysis where the duty cycle involves collecting: 1) an MS1 scan in the Orbitrap at 120,000 resolution across 350-1350 m/z range with automatic gain control (AGC) target of 1.0e6, 50 ms maximum injection time; 2) data dependent ion trap MS2 scans on the top 10 peptides with CID activation, 0.5 m/z isolation window in quadrupole, turbo scan rate, 2.0e4 AGC target, 100 ms maximum injection time; and 3) Orbitrap SPS-MS3 scans of 8 MS2 fragment ions, with isolation widths of 2 m/z using isolation waveforms with multiple frequency notches as described previously (30). MS3 precursor ions were fragmented by high energy collision-induced dissociation and analyzed by Orbitrap at 50,000 resolution, AGC target 2.5e5, 150 ms maximum injection time.

Data analysis for global and phospho-proteome multiplexed proteomics.

MS/MS spectra were searched using the Mascot algorithm (Matrix Sciences) against a concatenated target-decoy database comprised of the UniProt Mus musculus protein sequences (downloaded June 2016), known contaminants, and the reversed versions of each sequence. A 50 ppm precursor ion mass tolerance and 0.8 Da fragment ion tolerant were used with tryptic specificity, and up to 2 missed cleavages permitted. Fixed modifications were considered for carbamidomethylated cysteine residues (+57.0215 Da) and the TMT modification of the N-terminus and K residues (+229.1629 Da). Variable modifications were permitted for methionine oxidation (+15.9949 Da), phosphorylation on S/T/Y (+79.9663 Da) and TMT modification of Y (+229.1629 Da). Search results were filtered to 1% FDR at the peptide level and 2% FDR at the protein level using in house tools as described previously (28). Phospho-sites on peptides were localized with Ascore (31) and all peptides spanning phospho-sites were grouped using their residue and position nomenclature prior to modeling. MS3 based TMT quantification was performed using our in-house Mojave module (32), filtering out TMT peaks in MS3 scans whose reporter ion intensity sum < 30,000, across all 11 channels. For each peptide, the respective reporter ion intensities were summed across PSMs. Sequences <7 residues were further removed due to ambiguity in peptide to protein mapping. Then, for each protein or phospho-site, a model was fitted in MSstats v3.7.1 (33) using Tukey Median Polish summary on all quantified peptides across replicates with imputation of missing values below a censoring threshold of 2^8. Within MSstats, the model estimated fold change and statistical significance were computed for all compared treatment groups. Significantly altered proteins or phospho-sites were determined by setting a threshold of |Log2(fold-change)| > 1 and p-value < 0.05. The subset of significantly altered phospho-sites, unaltered at the protein level, was then annotated and tested for over-

222 represented biological annotations using the MsigDB collection and GSEA (34). Significant
223 annotations were defined by an enrichment q-value < 0.05.
224
225 **Lentivirus and PEG10 VLP generation.**
226 HEK293T cells (10^7) plated on gelatin-coated 10 cm dishes were transfected with 5 μg pGCMV-
227 MCS-IRES-eGFP (Genentech), Delta 8.9 or Delta 8.9-PEG10 (PEG10 residues 1-377 were cloned
228 into the p24 region of the Delta 8.9 vector), and VSV-G at a molar ratio of 1:2.3:0.2 using
229 Lipofectamine 2000 (Thermo Fisher). Media was replenished 6 h post-transfection and the
230 supernatant collected after a further 40 h. Lentivirus particles or VLPs were isolated using a Lenti-
231 X Concentrator (321231, Clontech).
232
233 **Protease protection assay.**
234 Lentiviruses and PEG10 VLPs were resuspended in PBS. Half of the sample was incubated with
235 1% Triton X-100, 0.5% TriButyl, and 0.2% SDS, and sonicated briefly to permeabilize the lipid
236 bilayer. 1 μg trypsin (V511A, Promega) was added to both samples (-/+ Triton) and incubated for
237 0, 30, 60, and 120 min on ice. Trypsinization was stopped by adding 5 mM PMSF. Samples were
238 boiled for 10 min in NuPAGE LDS Sample Buffer (NP0008, Thermo Fisher) and NuPAGE
239 Sample Reducing Agent (NP0004, Thermo Fisher).
240
241 **Vesicle isolation.**
242 Culture supernatants were centrifuged at 1500 x g, then 10,000 x g, and then filtered through a
243 0.22 μm vacuum filter unit. Further centrifugation at 100,000 x g for 2 h yielded a vesicle-
244 containing pellet. For sucrose gradient purification, the pellet was resuspended in 60% sucrose in

20 mM Tris-HCl pH 7.4 and 0.85% NaCl. This suspension was layered with 40% and 20% sucrose in 20 mM Tris-HCl pH 7.4 and 0.85% NaCl, and centrifuged at 150,000 x g for 14 h.

Microscopy.

For immuno-electron microscopy, vesicles were adsorbed onto formvar/carbon-coated grids for 20 min, and then fixed and permeabilized for 30 min with 4% paraformaldehyde (PFA) in PBS containing 5% Triton X-100. Samples were quenched in PBS/glycine, rinsed in PBS, and labeled for 1 h with 20 µg/mL anti-PEG10 antibody diluted in EM blocking solution (EMS, Aurion). Samples were washed in PBS for 15 min, and then incubated for 1 h with goat anti-rat 6 nm gold conjugate (Jackson ImmunoResearch) diluted 1/10 in EM blocking solution. Samples were washed in PBS for 10 min, rinsed in water, and stained with 2% ammonium molybdate for 30 sec. Samples were imaged with JEOL JEM-1400 TEM, Ultrascan 1000 CCD camera. For negative stain microscopy, samples were adsorbed to grids for 20 min, rinsed with water, and stained with 1% uranyl acetate for 60 sec.

Immunohistochemistry.

Sections of formalin-fixed, paraffin-embedded C57BL/6J mouse tissues (5 µm) were baked for 20 min at 70°C. Deparaffinization and hydration was performed in a Leica Autostainer XL (Leica Biosystems). Sections were quenched in 3% H_2O_2 for 4 min, blocked using a ScyTek Blocking Kit (BBK120, ScyTek Laboratories), and then incubated in 10% donkey serum in 3% BSA/PBS for 30 min. Labeling was for 1 h with 5 µg/ml anti-PEG10 antibody or IgG2b isotype control (553986, BD Pharmingen) in PBS containing 10% donkey serum and 3% BSA, followed by 30 min with 5 µg/ml biotinylated donkey anti-rat antibody (712-065-153, Jackson Laboratories).

Sections were treated with Vectastain ABC Elite Reagent (PK-6100, Vector Labs) and then incubated with Pierce Metal Enhanced DAB (3406, Thermo Fisher) for 5 min. Counterstaining was with Mayers filtered hematoxylin.

Immunofluorescence labeling.

Cells were fixed with 8% PFA, blocked for 1 h with 10% donkey serum, 2% BSA, and 0.2% saponin in PBS, incubated overnight at 4℃ in 5 µg/ml anti-PEG10 antibody in blocking buffer, and then for 1 h at room temperature in 2 µg/mL Alexa 488-conjugated donkey anti-rat antibody (A-21208, Thermo Fisher). Slides were mounted with ProLong Gold containing DAPI (P36931, Thermo Fisher). Confocal images were captured with a LEICA SP5 laser-scanning confocal microscope.

RNA sequencing.

Total RNA was extracted using a RNeasy Mini Kit (Qiagen), quantified in a NanoDrop 8000 (ThermoFisher), and assessed for integrity using both 2100 5 Bioanalyzer and 2200 TapeStation (Agilent). Libraries were prepared from 1 µg of total RNA with TruSeq RNA Sample Preparation Kit v2 (Illumina). Library size was confirmed using 2200 TapeStation and High Sensitivity D1K screen tape (Agilent), and concentration was determined by Library quantification kit (KAPA). Libraries were multiplexed five per lane and sequenced in a HiSeq2500 (Illumina) to generate 50 million paired end 75 bp reads. Filtering of fastq sequence files removed poor quality reads (read length < 18 or > 30% of cycles with Phred score < 23). Raw FASTQ reads were aligned to the mouse reference genome (GRCm38-mm10) using GSNAP (with parameters -M 2 -n 10 -B 2 -i 1 -N 1 -w 200000 -E 1 -- pairmax-rna=200000 --clip-overlap). Reads were filtered to include only

291 the uniquely mapped reads. Differential expression analysis was performed using the voom/limma
292 R package (35). Genes were considered differentially expressed if the log2 fold change was > 1
293 or < -1, and adjusted p-value < 0.05. Pathway analysis was performed with the R package EGSEA
294 (36).
295
296 **eCLIP**
297 eCLIP was performed by Eclipse BioInnovations Inc (San Diego) essentially as described (37). In
298 brief, $2x10^7$ TSCs were UV (254 nm)-crosslinked at 0.4 J/cm^2, snap frozen, and then lysed prior
299 to treatment with RNase I. PEG10 was immunoprecipitated with anti-PEG10 antibody pre-
300 coupled to sheep anti-mouse Dynabeads (Thermo Fisher) overnight at 4ºC. 20% of the sample
301 was used for western blotting, 2% was used as a paired input, and the remainder was processed for
302 eCLIP. Raw FASTQ files were trimmed of 3' barcodes and adapter sequences. Reads were
303 aligned to the mouse reference genome (GRCm38-mm10) using STAR {Dobin, 2013 #1496}
304 followed by removal of PCR duplicates and reads mapping to repetitive elements in the genome.
305 MACS2 {Zhang, 2008 #1426} was used to call peaks in wild-type samples using PEG10-deficient
306 samples as controls. In Fig 7B, each PEG10 bound gene was divided into 100 bins between the
307 Transcription Start Site (TSS) and the Transcription End Site (TES), and into 20 bins upstream
308 and downstream of TSS and TES, respectively. For each bin, count of 5'-end of each eCLIP read
309 was calculated and summed across all genes to create the average profile per sample. All samples
310 were normalized to sequencing depth.
311

Raw data deposition.

All mass spectrometry raw files were uploaded on the Massive data repository and can be downloaded from ftp://MSV000083229@massive.ucsd.edu (login: MSV000083229_reviewer, password: a). eCLIP and RNAseq data have been deposited to the Gene Expression Omnibus (GEO accession number GSE122217). Data can be accessed using the token "kpmneycydrcvdat".

RESULTS AND DISCUSSION

PEG10 is regulated by USP9X.

We identified PEG10 while looking for substrates of the deubiquitinating enzyme USP9X in mouse ESCs. USP9X was affinity purified from *Usp9x*$^{3xf/y}$ ESCs, which had a 3xFLAG epitope tag inserted in frame with the N-terminus of USP9X. Co-immunoprecipitating proteins captured with anti-FLAG antibody and identified by mass spectrometry included PEG10 (Fig 1A). We confirmed that both PEG10-RF1 and PEG10-RF1/2 also interacted with untagged USP9X using *Peg10*$^{+/3xf}$ *Usp9x* *Rosa26*$^{+/CreERT2}$ ESCs, which delete *Usp9x* in response to 4-hydroxytamoxifen and express PEG10 proteins tagged at the N-terminus with 3xFLAG. Importantly, a USP9X antibody co-immunoprecipitated 3xFLAG.PEG10-RF1 and 3xFLAG.PEG10-RF1/2 only when the ESCs expressed USP9X (Fig 1B). Ubiquitin-substrate profiling by K-ε-GG mass spectrometry (38) revealed PEG10 as a putative substrate of USP9X because *Usp9x*$^{C1599A/y}$ ESCs expressing catalytically inactive USP9X C1599A (Fig 1C) contained more ubiquitinated PEG10 than wild-type ESCs (Fig 1, D-F). PEG10 deubiquitination by USP9X appeared to stabilize PEG10-RF1 specifically because USP9X-deficient ESCs contained less PEG10-RF1 than control ESCs, whereas the amount of PEG10-RF1/2 was largely unaltered (Fig 1, B and G). Consistent with ubiquitinated PEG10-RF1 being targeted for proteasomal

degradation, the proteasome inhibitor MG-132 increased the amount of PEG10-RF1 in USP9X-deficient ESCs, but had little impact on PEG10-RF1/2 (Fig 1G). PEG10-RF1 has six unique residues that are located in the frameshift region and are not found in PEG10-RF1/2 (12), so these may contribute to a degron motif that specifies its proteasomal degradation. We did not detect any ubiquitination sites within the frameshift region, but USP9X suppressed ubiquitination of two adjacent lysines (K365, K362). Whether mutation of these lysines impacts PEG10-RF1 stability is an area of future investigation.

Fig 1. PEG10 is a substrate of USP9X.

(A) USP9X interaction network showing all high confidence binding partners connected by solid lines (Saint > 0.9, FDR < 0.05, Avg. Psms > 10). Dotted lines indicate interactions reported in the BioPlex network (50, 51). Results are representative of 3 independent experiments. (B) Western blots of *Peg10*$^{3xf/+}$ *Usp9X*$^{fl/y}$ *Rosa26*.CreER^{T2} ESCs after immunoprecipitation (IP) of USP9X. Epitope-tagged PEG10 was detected with anti-FLAG antibody. Where indicated, ESCs were treated with 4-hydroxytamoxifen (4-OHT) to delete *Usp9x*. Results are representative of 2 independent experiments. (C) Western blots of ESCs. (D) Geyser plot showing proteins differentially ubiquitinated in *Usp9x*$^{C1566A/y}$ ESCs versus control *Usp9x*$^{+/y}$ ESCs ($p < 0.05$, $\log_2$ fold change > 2). Results are representative of 2 independent experiments. (E) Line plot showing the fold-change in abundance of all ubiquitinated PEG10 peptides between *Usp9x*$^{+/y}$ and *Usp9x*$^{C1566A/y}$ ESCs. Each grey line corresponds to a unique KGG peptide spectral match peptide. The red line indicates a model-based protein abundance estimate. AUC, area under the curve.

(F) Diagram indicating the position of the USP9X-regulated ubiquitination (Ub) sites in PEG10. Triangles depict ubiquitination sites identified only in *Usp9x*$^{C1566A/y}$ ESCs. Circles depict sites found in *Usp9x*$^{+/y}$ and *Usp9x*$^{C1566A/y}$ ESCs. Circle size indicates the extent to which ubiquitination was increased by USP9X inactivation. (G) Western blots of *Peg10* $^{3xf/+}$ *Usp9x*$^{fl/y}$ *Rosa26*.CreER^{T2} ESCs. Where indicated, cells were treated with 10 μM MG-132 for 4 h. Results are representative of 2 independent experiments.

The PEG10 Gag domain forms virus-like particles.

The biochemical roles of PEG10 are unknown. The Gag polyproteins of Ty3 retrotransposons have been shown to assemble virus-like particles (VLPs) (39), so we explored whether the conserved PEG10 Gag domain could substitute for the p24 HIV-1 Gag protein in a lentiviral packaging system. HEK293T cells were co-transfected with VSV-G envelope protein and either HIV-1 Gag-Pol or a hybrid construct encoding PEG10-RF1 and HIV-1 Pol. Both p24 and PEG10-RF1 were detected in the culture supernatant by western blotting (Fig 2A), suggesting that both Gags assembled VLPs. Sucrose gradient centrifugation suggested the putative PEG10-RF1 VLPs were denser than the HIV-1 p24 VLPs (Fig 2B). VLPs that bud from the cell are encapsulated in a lipid bilayer that protects Gag proteins from digestion with trypsin. Accordingly, PEG10-RF1 in culture supernatants was only cleaved by trypsin in the presence of the bilayer-disrupting detergent Triton X-100 (Fig 2C). Indeed, lipid bilayer-encapsulated PEG10-RF1 VLPs were detected by negative stain electron microscopy (Fig. 2D).

Fig 2. The PEG10 Gag domain generates virus-like particles.

(A) Western blots of HEK293T cells or extracellular vesicles recovered from the culture medium after transfection with VSV-G and increasing amounts of Gag-Pol cDNA. Results are representative of 2 independent experiments. (B) Western blots of extracellular vesicles in panel A after sucrose gradient density centrifugation. The upper blot shows cells transfected with HIV-1 Gag, whereas the lower blot shows cells transfected with PEG10-RF1. We speculate that the faster migrating PEG10-RF1 species is a processed form of the protein. Results are representative of 2 independent experiments. (C) Western blots of VLPs. Results are representative of 3 independent experiments. (D) Electron micrographs of negatively stained VLPs. Scale bar, 20 nm. Results are representative of 2 independent experiments. (E) Western blots of wild-type ESCs and TSCs. Results are representative of 2 independent experiments. (F) Western blots of HEK293T cells ectopically expressing wild-type (WT) mouse PEG10 or a PEG10 frameshift (FS) mutant that can only make PEG10-RF1/2. Results are representative of 2 independent experiments. (G) Western blots of extracellular vesicles shed from WT or PEG10-deficient (KO) TSCs and enriched by differential centrifugation. Results are representative of 5 independent experiments. (H) Western blots of extracellular vesicles shed from WT TSCs and analyzed by sucrose gradient density centrifugation. Results are representative of 2 independent experiments. (I) Electron micrographs of TSC extracellular vesicles after immuno-gold labeling for PEG10. Scale bar, 50 nm.

Next, we determined if endogenous PEG10 was in vesicles shed from trophoblast stem cells (TSCs), which express even more PEG10 than ESCs (Fig 2E). PEG10 was detected with a monoclonal antibody that was raised against PEG10-RF1, and therefore detects both PEG10-RF1 and PEG10-RF1/2 (Fig 2, E and F). We found that both PEG10-RF1 and PEG10-RF1/2 were

present in supernatant fractions enriched for TSC extracellular vesicles (Fig 2, G and H). The exosome marker TSG101 (40) served as a positive control. Electron microscopy and immuno-gold labeling for PEG10 confirmed the presence of PEG10-bearing vesicles (Fig 2I). Collectively, our data suggest that the PEG10 Gag domain supports constitutive VLP assembly.

To investigate the mechanism of PEG10 budding, we affinity purified PEG10 from ESCs and TSCs and then identified co-immunoprecipitating proteins by mass spectrometry (Fig 3A). Consistent with our previous experiments, PEG10 interacted with USP9X and USP9X-associated proteins such as ATXN10, IQCB1, BAG6 and UBL4. Intriguingly, two proteins involved in vesicle fusion, VTI1B and STX8 (41, 42), also coimmunoprecipitated with PEG10 (Fig 3, A and B). It is tempting to speculate that VTI1B and STX8 might regulate the budding of PEG10-containing vesicles.

Fig 3. Proteins interacting with PEG10 in ESCs and TSCs.

(A) PEG10 interaction network showing all high confidence binding partners connected by solid lines (Saint > 0.9, FDR < 0.05, Avg. Psms > 10). Dotted lines indicate interactions reported in the Bioplex interaction network. Proteins co-immunoprecipitated from both TSCs and ESCs are colored red, and those unique to ESCs are green. Results are representative of 3 independent experiments. (B) Western blots before and after immunoprecipitation (IP) of 3xFLAG.PEG10 from knock-in ESCs, or as a control, PEG10-deficient (KO) ESCs. Results are representative of 2 independent experiments.

PEG10 is expressed in a subset of adult mouse tissues.

PEG10 has been studied largely in developmental settings and in cancer cell lines, so we determined its expression in a broad panel of mouse tissues. PEG10-RF1 and PEG10-RF1/2 were both abundant in adrenal gland, testis and placenta, whereas pituitary, ovary, uterus, white adipose, brain and lung expressed them to a lesser extent (Fig 4A). Additional faster migrating bands detected by the PEG10 antibody may reflect proteolytic processing of PEG10. Immunolabeling of tissue sections revealed that PEG10 was expressed highly in the cortex of the adrenal gland, the pars distalis of the pituitary gland, the sertoli cells of the testis, the hypothalamus, and in the labyrinth and trophoblast layers of the placenta (Fig 4B). Expression of PEG10 in the pituitary gland is interesting given that PEG10-deficient mice generated by tetraploid complementation exhibit severe growth retardation (13). PEG10 appeared largely cytoplasmic in the different mouse tissues. Immunofluorescence staining (Fig 4C) and biochemical fractionation studies (Fig. 4D) indicated that PEG10 in ESCs and TSCs was also mostly cytoplasmic. Both PEG10-RF1 and PEG10-RF1/2 were in the cytoplasm of ESCs, but some PEG10-RF1/2 was nuclear in TSCs (Fig. 4D). Therefore, the cellular localization of PEG10 appears context-dependent.

Figure 4. Expression of PEG10 in mouse tissues.

(A) Western blots of C57BL/6 mouse tissues. Results are representative of 3 independent experiments. (B) Mouse tissue sections immunolabeled for PEG10 (brown). AC, adrenal cortex. AM, adrenal medulla. LN, Labyrinth. T, Trophoblast. DB, decidua basalis. ST, Sertoli cells. LC, Leydig cells. PN, pars nervosa. PI, pars intermedia. PD, pars distalis. Th, thalamus. Hyp, Hypothalamus. Scale bar, 100 μm. Results are representative of 3 independent experiments. (C) Immunofluorescence staining of PEG10 in ESCs or TSCs. Scale bar, 25 μm. Results are representative of 2 independent experiments. (D) Western blots of ESCs and TSCs that were

fractionated into cytoplasmic (cyto) and nuclear (nuc) compartments. Results are representative of 3 independent experiments.

PEG10 is essential for TSC differentiation.

PEG10 is essential for formation of the labyrinth and spongiotrophoblast layers of the placenta (13). TSCs isolated from the early blastocyst can be differentiated into cells of the labyrinth and spongiotrophoblast layers (25), so we utilized this culture system to further explore the function of PEG10. TSCs were maintained in their pluripotent state on CELLstart extracellular matrix in the presence of fibroblast growth factor 4 (Fgf4) and heparin, or they were differentiated in the absence of CELLstart, Fgf4, and heparin in either 20% oxygen, to form the multinucleated syncytiotrophoblasts (SynTs) of the labyrinth, or 2% oxygen, to form the spongiotrophoblasts and trophoblast giant cells (TGCs) of the junctional zone. We noted that expression of PEG10-RF1/2 and PEG10-RF1 increased as TSCs were differentiated in 20% oxygen (Fig 5A). Upregulation of PEG10 was functionally significant because CRISPR-Cas9-mediated deletion of *Peg10* (Fig. 4D) impaired TSC differentiation under both normoxic and hypoxic conditions (Fig 5, B and C). Morphologically, PEG10-deficient cells retained an undifferentiated appearance (Fig 5B), and by RNA sequencing (RNA-seq), they failed to manifest the transcriptional signature of wild-type, differentiated TSCs (Fig 5C; data available in full through the GEO database, accession GSE122217).

Figure 5. PEG10 regulates the differentiation of TSCs.

(A) Western blots of TSCs differentiated in 20% oxygen for the times indicated. *Peg10* mRNA expression was determined by quantitative RT-PCR. (B) Micrographs of wild-type (WT) and

PEG10-deficient (KO) TSCs. Results are representative of 5 independent experiments. (C) Principal Component Analysis (PCA) of TSC RNA-seq datasets using log2 RPKM values.

Global proteome and phospho-serine/-threonine/-tyrosine profiling revealed many differences between wild-type and PEG10-deficient TSCs following differentiation (Fig 6, A-D). One particularly interesting difference was the altered phospho-status of key signaling proteins such as MAPK1, MAPK3, MTOR, INSR, and EGFR (Fig 6, B and E). Indeed, enrichment analysis of differentially phosphorylated proteins highlighted aberrant MTOR, Insulin, ErbB, and MAPK signaling (Fig 6F). Phosphoproteome analysis also allowed us to map phospho-sites within PEG10 (Fig 6G).

Fig 6. Proteomic analysis of wild-type and PEG10-deficient TSCs.

(A and B) Volcano plots of total protein levels (A) or phosphorylation levels at unique phosphosites (B) in wild-type (WT) versus PEG10-deficient (KO) TSCs after 0 and 5 days of differentiation. Results are representative of 3 independent experiments. (C) Venn diagram indicates the total number of proteins identified and quantified by global proteome profiling (GPP) and phosphoproteome profiling (pSTY). (D) Fraction of proteins (GPP) or phosphosites on Ser/Thr/Try (pSTY) with levels changing more than 2-fold (p-value <= 0.05) in PEG10 KO TSCs compared to WT TSCs after 0 and 5 days of differentiation. (E) Western blots of WT and PEG10 KO TSCs after 0 and 9 days of differentiation. (F) Pathways highlighted by the Broad Institute gene set enrichment analysis of proteins with significantly changing phosphorylation levels in PEG10 KO TSCs compared to WT TSCs. (G) Diagram indicates the position of phosphosites in PEG10.

493

494 **PEG10 binds to cellular RNAs.**

495 The PEG10 Gag domain harbors a conserved zinc finger (ZnF) motif (12) that is reminiscent of
496 the ZnF motifs in orthoretroviral Gags for binding and packaging nucleic acids (43). Therefore,
497 we performed eCLIP-seq (enhanced crosslinking and immunoprecipitation - sequencing) (37) on
498 wild-type and PEG10-deficient TSCs to determine if PEG10 was an RNA binding protein. PEG10
499 interacted with the 3' untranslated regions (UTRs) of approximately 840 and 3,680 unique mRNAs
500 after zero and five days of differentiation (normoxic conditions), respectively (Fig 7, A and B; data
501 available in full through the GEO database, accession GSE122217). However, these 3' UTRs did
502 not have any RNA sequence motifs in common (Fig 7C), which could indicate that RNA secondary
503 structure determines PEG10 binding. PEG10 was bound to its own mRNA (Fig 7D) and to RNAs
504 encoding kinases (MAPK1, MAP2K1, GSK3β, ROCK1, and ROCK2) and regulators of signaling
505 pathways (CMKLR1, TGFα, CBL, GAB1, and HBEGF). Our RNA-seq dataset revealed that a
506 large number of PEG10-bound transcripts, including *Hbegf* (heparin-binding EGF-like growth
507 factor), showed increased expression in wild-type TSCs after differentiation but did not increase
508 in PEG10-deficient TSCs (Fig 7, D and E). HBEGF protein was also less abundant in PEG10-
509 deficient TSCs than in WT TSCs after 5 days of differentiation (Fig 6A). *Hbegf* stood out in this
510 list of genes because of its important role in placentation (44). Therefore, RNA binding by PEG10
511 appears to promote the expression of genes necessary for differentiation of the placental lineages.

512

513 **Fig 7. PEG10 binds to RNA.**

514 (A) Venn diagram showing RNA transcripts bound to PEG10 after 0 and 5 days of differentiation
515 under normoxic conditions. (B) Graph indicates the distribution of 5'-end eCLIP reads after

516 immunoprecipitating PEG10 from wild-type (WT) and PEG10-deficient (KO) TSCs. Reads are
517 normalized to sequencing depth. (C) Diagram indicates the percentage distribution of nucleotides
518 in PEG10-bound and unbound 3' UTRs. (D) eCLIP-seq data from WT and PEG10 KO TSCs.
519 Blue boxes at the top indicate the location of the genes. (E) Scatter plot comparing RNA-seq and
520 eCLIP peak scores from WT and PEG10 KO TSCs. Genes are shaded red if they are up-regulated
521 in WT TSCs by RNA-seq (log2 fold change >1 and p-value <0.05), grey if they are unchanged
522 (log2 fold change <1 or >-1), and green if they are down-regulated in WT TSCs (log2 fold change
523 <-1 and p-value <0.05). Results are representative of 2 independent experiments.
524
525 In summary, despite its domestication, *Peg10* maintains several hallmarks of retroviral and
526 retrotransposon Gag proteins. The Gag domain of PEG10 supports the budding of virus-like
527 particles, which are released from the cell and can be recovered from exosome preparations. ARC
528 (activity regulated cytoskeletal-associated protein) is another retroviral-like Gag protein that drives
529 the budding of extracellular vesicles (46, 47). ARC, like PEG10, binds to its own mRNA. The
530 release and uptake of *Arc*-containing VLPs by neurons is considered a mechanism of intercellular
531 communication (46, 47). Additional work is needed to determine if PEG10 fulfils a similar
532 function.
533
534 **ACKNOWLEDGMENTS**
535 PTMscan® is performed at Genentech under limited license from Cell Signaling Technologies
536 (Danvers, MA). We thank Ben Haley for reagents; Woong Kim and Daisy Bustos for technical
537 assistance.
538

REFERENCES

1. Platt RN, 2nd, Vandewege MW, Ray DA. Mammalian transposable elements and their impacts on genome evolution. Chromosome Res. 2018;26: 25-43.

2. Konkel MK, Batzer MA. A mobile threat to genome stability: The impact of non-LTR retrotransposons upon the human genome. Semin Cancer Biol. 2010;20: 211-221.

3. Kidwell MG, Lisch D. Transposable elements as sources of variation in animals and plants. Proc Natl Acad Sci U S A. 1997;94: 7704-7711.

4. Le Rouzic A, Boutin TS, Capy P. Long-term evolution of transposable elements. Proc Natl Acad Sci U S A. 2007;104: 19375-19380.

5. Yoder JA, Walsh CP, Bestor TH. Cytosine methylation and the ecology of intragenomic parasites. Trends Genet. 1997;13: 335-340.

6. Volff JN. Turning junk into gold: domestication of transposable elements and the creation of new genes in eukaryotes. Bioessays. 2006;28: 913-922.

7. Mi S, Lee X, Li X, Veldman GM, Finnerty H, Racie L, et al. Syncytin is a captive retroviral envelope protein involved in human placental morphogenesis. Nature. 2000;403: 785-789.

8. Kaneko-Ishino T, Ishino F. The role of genes domesticated from LTR retrotransposons and retroviruses in mammals. Front Microbiol. 2012;3: 262.

9. Grow EJ, Flynn RA, Chavez SL, Bayless NL, Wossidlo M, Wesche DJ, et al. Intrinsic retroviral reactivation in human preimplantation embryos and pluripotent cells. Nature. 2015;522: 221-225.

10. Malik HS. Retroviruses push the envelope for mammalian placentation. Proc Natl Acad Sci U S A. 2012;109: 2184-2185.

562 11. Ono R, Kobayashi S, Wagatsuma H, Aisaka K, Kohda T, Kaneko-Ishino T, et al. A
563 retrotransposon-derived gene, PEG10, is a novel imprinted gene located on human chromosome
564 7q21. Genomics. 2001;73: 232-237.
565 12. Clark MB, Janicke M, Gottesbuhren U, Kleffmann T, Legge M, Poole ES, et al.
566 Mammalian gene PEG10 expresses two reading frames by high efficiency -1 frameshifting in
567 embryonic-associated tissues. J Biol Chem. 2007;282: 37359-37369.
568 13. Ono R, Nakamura K, Inoue K, Naruse M, Usami T, Wakisaka-Saito N, et al. Deletion of
569 Peg10, an imprinted gene acquired from a retrotransposon, causes early embryonic lethality.
570 Nature genetics. 2006;38: 101-106.
571 14. Okabe H, Satoh S, Furukawa Y, Kato T, Hasegawa S, Nakajima Y, et al. Involvement of
572 PEG10 in human hepatocellular carcinogenesis through interaction with SIAH1. Cancer Res.
573 2003;63: 3043-3048.
574 15. Akamatsu S, Wyatt AW, Lin D, Lysakowski S, Zhang F, Kim S, et al. The Placental
575 Gene PEG10 Promotes Progression of Neuroendocrine Prostate Cancer. Cell Rep. 2015;12: 922-
576 936.
577 16. Ramalho-Santos M, Yoon S, Matsuzaki Y, Mulligan RC, Melton DA. "Stemness":
578 transcriptional profiling of embryonic and adult stem cells. Science. 2002;298: 597-600.
579 17. Ivanova NB, Dimos JT, Schaniel C, Hackney JA, Moore KA, Lemischka IR. A stem cell
580 molecular signature. Science. 2002;298: 601-604.
581 18. Van Hoof D, Passier R, Ward-Van Oostwaard D, Pinkse MW, Heck AJ, Mummery CL,
582 et al. A quest for human and mouse embryonic stem cell-specific proteins. Mol Cell Prot.
583 2006;5: 1261-1273.

584 19. Naik E, Webster JD, DeVoss J, Liu J, Suriben R, Dixit VM. Regulation of proximal T
585 cell receptor signaling and tolerance induction by deubiquitinase Usp9X. J Exp Med. 2014;211:
586 1947-1955.
587 20. Schwickart M, Huang X, Lill JR, Liu J, Ferrando R, French DM, et al. Deubiquitinase
588 USP9X stabilizes MCL1 and promotes tumour cell survival. Nature. 2010;463: 103-107.
589 21. Naik E, Dixit VM. Usp9X Is Required for Lymphocyte Activation and Homeostasis
590 through Its Control of ZAP70 Ubiquitination and PKCbeta Kinase Activity. J Immunol.
591 2016;196: 3438-3451.
592 22. Xie Y, Avello M, Schirle M, McWhinnie E, Feng Y, Bric-Furlong E, et al.
593 Deubiquitinase FAM/USP9X interacts with the E3 ubiquitin ligase SMURF1 protein and
594 protects it from ligase activity-dependent self-degradation. J Biol Chem. 2013;288: 2976-2985.
595 23. Khan OM, Carvalho J, Spencer-Dene B, Mitter R, Frith D, Snijders AP, et al. The
596 deubiquitinase USP9X regulates FBW7 stability and suppresses colorectal cancer. J Clin Invest.
597 2018;128: 1326-1337.
598 24. Seibler J, Zevnik B, Kuter-Luks B, Andreas S, Kern H, Hennek T, et al. Rapid generation
599 of inducible mouse mutants. Nucleic Acids Res. 2003;31: e12.
600 25. Choi HJ, Sanders TA, Tormos KV, Ameri K, Tsai JD, Park AM, et al. ECM-dependent
601 HIF induction directs trophoblast stem cell fate via LIMK1-mediated cytoskeletal rearrangement.
602 PloS one. 2013;8: e56949.
603 26. Choi H, Larsen B, Lin ZY, Breitkreutz A, Mellacheruvu D, Fermin D, et al. SAINT:
604 probabilistic scoring of affinity purification-mass spectrometry data. Nat Methods. 2011;8: 70-
605 73.

606 27. Bingol B, Tea JS, Phu L, Reichelt M, Bakalarski CE, Song Q, et al. The mitochondrial
607 deubiquitinase USP30 opposes parkin-mediated mitophagy. Nature. 2014;510: 370-375.
608 28. Kirkpatrick DS, Bustos DJ, Dogan T, Chan J, Phu L, Young A, et al. Phosphoproteomic
609 characterization of DNA damage response in melanoma cells following MEK/PI3K dual
610 inhibition. Proc Natl Acad Sci U S A.2013;110: 19426-19431.
611 29. Paulo JA, Gygi SP. Nicotine-induced protein expression profiling reveals mutually
612 altered proteins across four human cell lines. Proteomics. 2017;17. doi:
613 10.1002/pmic.201600319.
614 30. McAlister GC, Nusinow DP, Jedrychowski MP, Wuhr M, Huttlin EL, Erickson BK, et al.
615 MultiNotch MS3 enables accurate, sensitive, and multiplexed detection of differential expression
616 across cancer cell line proteomes. Anal Chem. 2014;86: 7150-7158.
617 31. Beausoleil SA, Villen J, Gerber SA, Rush J, Gygi SP. A probability-based approach for
618 high-throughput protein phosphorylation analysis and site localization. Nat Biotech. 2006;24:
619 1285-1292.
620 32. Zhuang G, Yu K, Jiang Z, Chung A, Yao J, Ha C, et al. Phosphoproteomic analysis
621 implicates the mTORC2-FoxO1 axis in VEGF signaling and feedback activation of receptor
622 tyrosine kinases. Sci Signal. 2013;6: ra25.
623 33. Choi M, Chang CY, Clough T, Broudy D, Killeen T, MacLean B, et al. MSstats: an R
624 package for statistical analysis of quantitative mass spectrometry-based proteomic experiments.
625 Bioinformatics. 2014;30: 2524-2526.
626 34. Subramanian A, Tamayo P, Mootha VK, Mukherjee S, Ebert BL, Gillette MA, et al.
627 Gene set enrichment analysis: a knowledge-based approach for interpreting genome-wide
628 expression profiles. Proc Natl Acad Sci U S A. 2005;102: 15545-15550.

629 35. Ritchie ME, Phipson B, Wu D, Hu Y, Law CW, Shi W, et al. limma powers differential
630 expression analyses for RNA-sequencing and microarray studies. Nucleic Acids Res. 2015;43:
631 e47.
632 36. Alhamdoosh M, Ng M, Wilson NJ, Sheridan JM, Huynh H, Wilson MJ, et al. Combining
633 multiple tools outperforms individual methods in gene set enrichment analyses. Bioinformatics.
634 2017;33: 414-424.
635 37. Van Nostrand EL, Pratt GA, Shishkin AA, Gelboin-Burkhart C, Fang MY, Sundararaman
636 B, et al. Robust transcriptome-wide discovery of RNA-binding protein binding sites with
637 enhanced CLIP (eCLIP). Nat Methods. 2016;13: 508-514.
638 38. Bustos D, Bakalarski CE, Yang Y, Peng J, Kirkpatrick DS. Characterizing ubiquitination
639 sites by peptide-based immunoaffinity enrichment. Mol Cell Prot. 2012;11: 1529-1540.
640 39. Finnegan DJ. Retrotransposons. Current biology : CB. 2012;22: R432-R437.
641 40. Willms E, Johansson HJ, Mager I, Lee Y, Blomberg KE, Sadik M, et al. Cells release
642 subpopulations of exosomes with distinct molecular and biological properties. Sci Rep. 2016;6:
643 22519.
644 41. Prekeris R, Yang B, Oorschot V, Klumperman J, Scheller RH. Differential roles of
645 syntaxin 7 and syntaxin 8 in endosomal trafficking. Mol Biol Cell. 1999;10:3891-3908.
646 42. Antonin W, Riedel D, von Mollard GF. The SNARE Vti1a-beta is localized to small
647 synaptic vesicles and participates in a novel SNARE complex. J Neurosci. 2000;20: 5724-5732.
648 43. Amarasinghe GK, De Guzman RN, Turner RB, Chancellor KJ, Wu ZR, Summers MF.
649 NMR structure of the HIV-1 nucleocapsid protein bound to stem-loop SL2 of the psi-RNA
650 packaging signal. Implications for genome recognition. J Mol Biol. 2000;301: 491-511.

651 44. Liu Z, Skafar DF, Kilburn B, Das SK, Armant DR. Extraembryonic Heparin-Binding
652 Epidermal Growth Factor-Like growth factor (HBEGF) deficiency compromises placentation in
653 mice. Biol Reprod. 2019;100: 217-226.
654 45. Campillos M, Doerks T, Shah PK, Bork P. Computational characterization of multiple
655 Gag-like human proteins. Trends Genet. 2006;22: 585-589.
656 46. Ashley J, Cordy B, Lucia D, Fradkin LG, Budnik V, Thomson T. Retrovirus-like Gag
657 Protein Arc1 Binds RNA and Traffics across Synaptic Boutons. Cell. 2018;172: 262-274.
658 47. Pastuzyn ED, Day CE, Kearns RB, Kyrke-Smith M, Taibi AV, McCormick J, et al. The
659 Neuronal Gene Arc Encodes a Repurposed Retrotransposon Gag Protein that Mediates
660 Intercellular RNA Transfer. Cell. 2018;172: 275-288.
661 48. D'Souza V, Melamed J, Habib D, Pullen K, Wallace K, Summers MF. Identification of a
662 high affinity nucleocapsid protein binding element within the Moloney murine leukemia virus
663 Psi-RNA packaging signal: implications for genome recognition. J Mol Biol. 2001;314: 217-232.
664 49. Jessmon P, Leach RE, Armant DR. Diverse functions of HBEGF during pregnancy. Mol
665 Reprod Dev. 2009;76: 1116-1127.
666 50. Huttlin EL, Ting L, Bruckner RJ, Gebreab F, Gygi MP, Szpyt J, et al. The BioPlex
667 Network: A Systematic Exploration of the Human Interactome. Cell. 2015;162: 425-440.
668 51. Huttlin EL, Bruckner RJ, Paulo JA, Cannon JR, Ting L, Baltier K, et al. Architecture of
669 the human interactome defines protein communities and disease networks. Nature. 2017;545:
670 505-509.
671

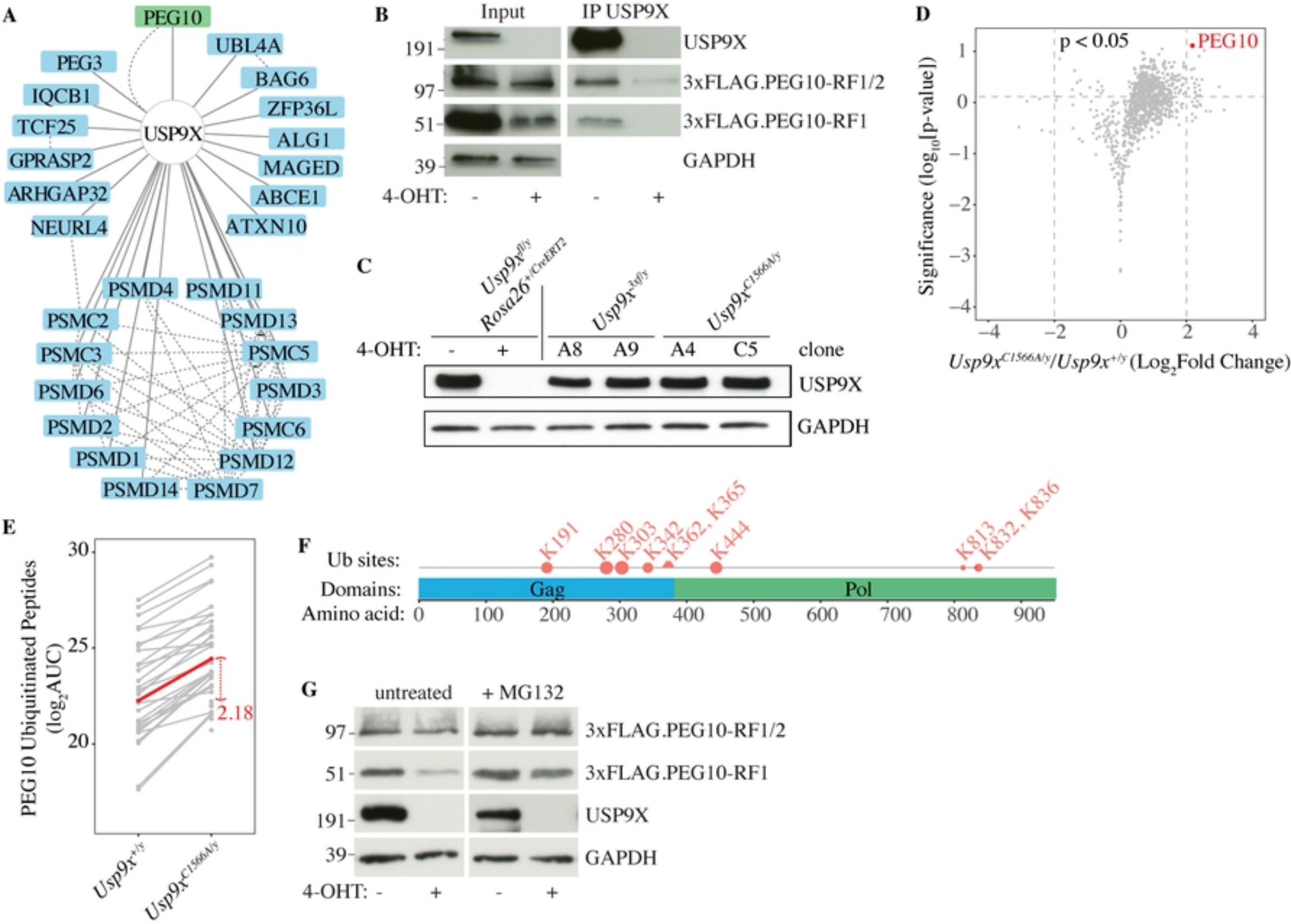
A
PEG10
UBL4A
PEG3
BAG6
IQCB1
ZFP36L
TCF25
USP9X
ALG1
GPRASP2
MAGED
ARHGAP32
ABCE1
NEURL4
ATXN10
PSMD4
PSMD11
PSMC2
PSMD13
PSMC3
PSMC5
PSMD6
PSMD3
PSMD2
PSMC6
PSMD1
PSMD12
PSMD14
PSMD7
B
Input
IP USP9X
191
97
51
39
USP9X
3xFLAG.PEG10-RF1/2
3xFLAG.PEG10-RF1
GAPDH
4-OHT: - + - +
C
Usp9x^flfy Rosa26^+/CreERT2
Usp9x^3dfy
Usp9x^C1566A/y
4-OHT: - + A8 A9 A4 C5
clone
USP9X
GAPDH
D
p < 0.05
PEG10
Significance (log10[p-value])
Usp9x^C1566A/y/Usp9x^+/y (Log2Fold Change)
E
PEG10 Ubiquitinated Peptides (log2AUC)
2.18
Usp9x^+/y
Usp9x^C1566A/y
F
Ub sites:
K191
K280
K303
K342
K362, K365
K444
K813
K832, K836
Domains:
Gag
Pol
Amino acid:
G
untreated
+ MG132
97
51
191
39
3xFLAG.PEG10-RF1/2
3xFLAG.PEG10-RF1
USP9X
GAPDH
4-OHT: - + - +

Figure 1

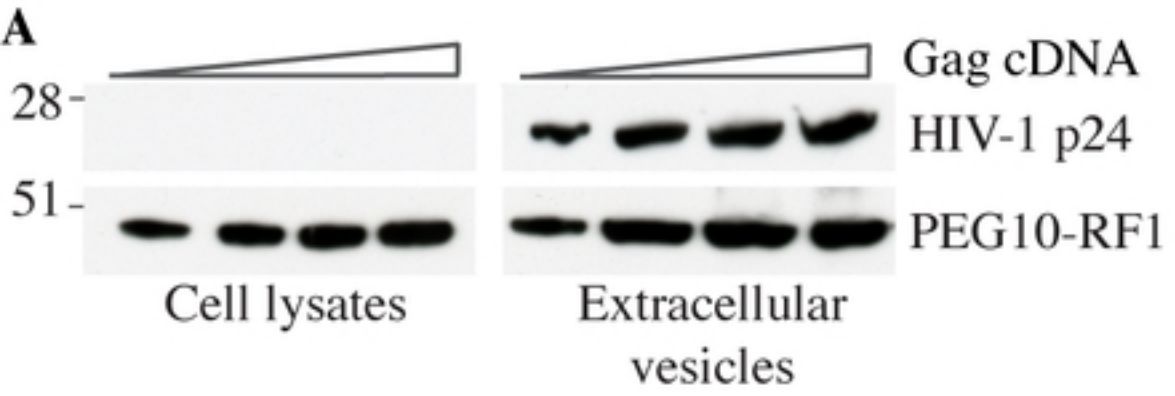

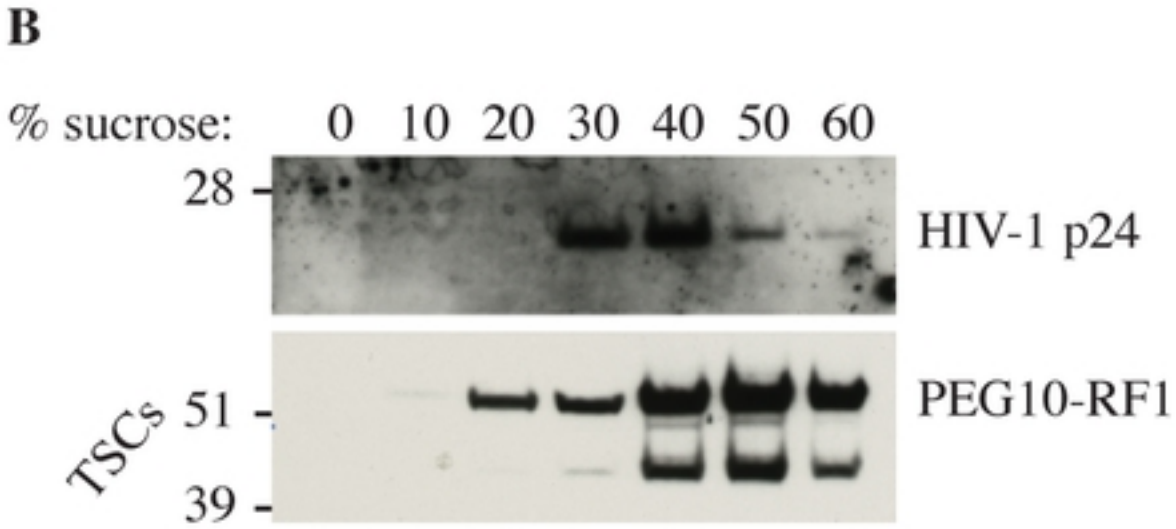

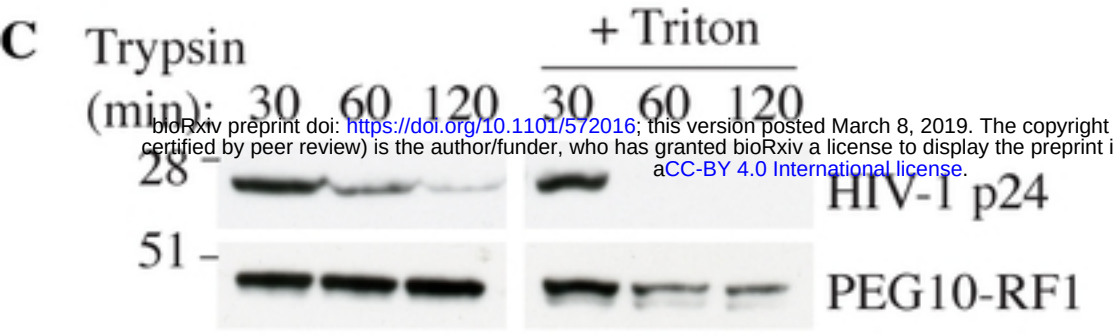

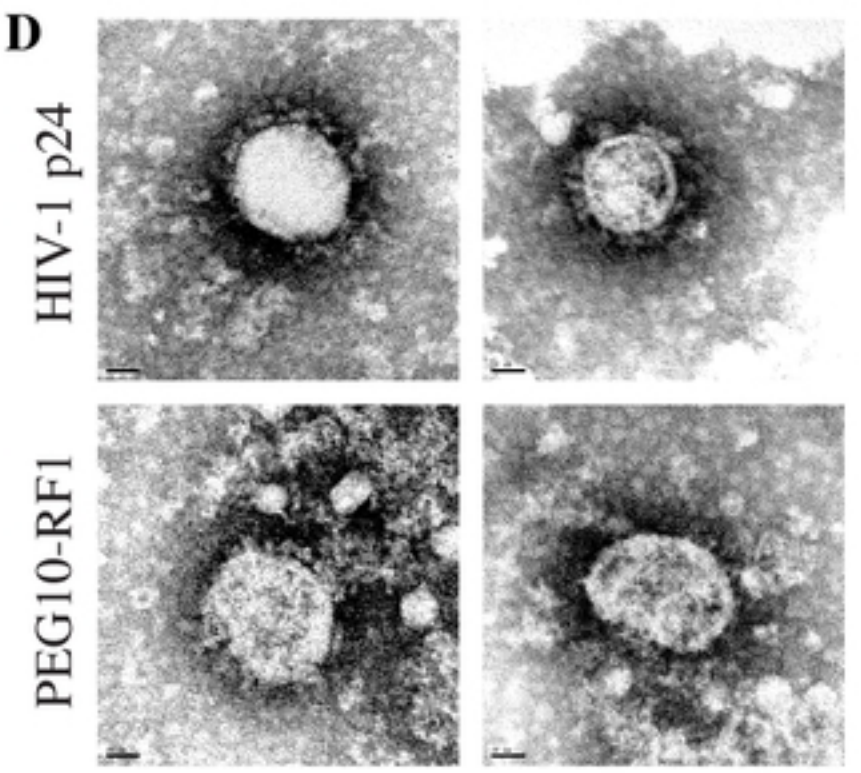

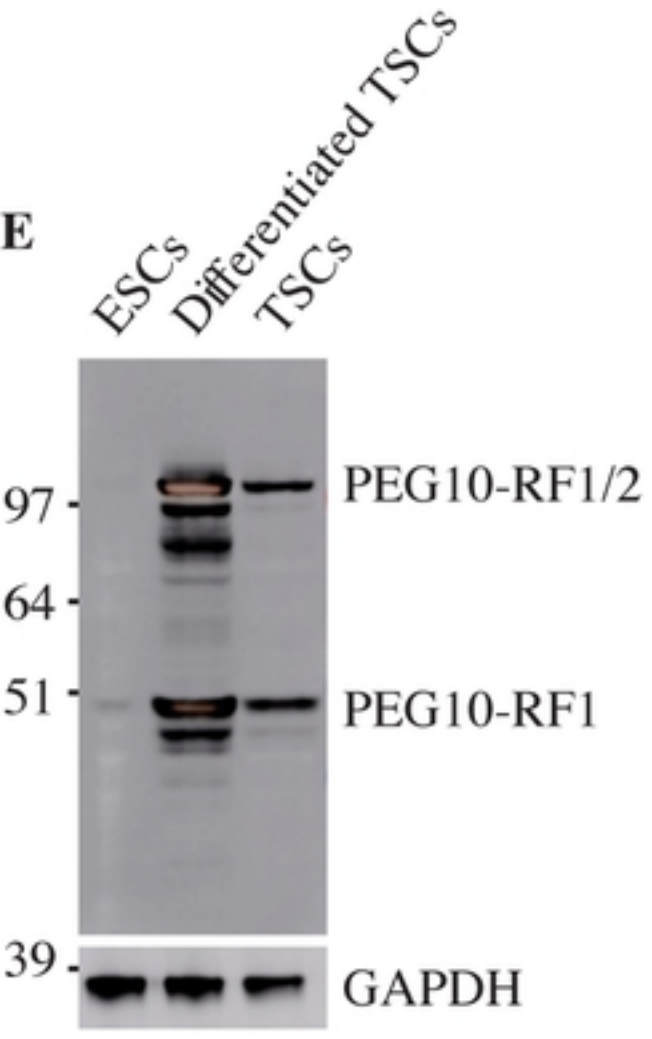

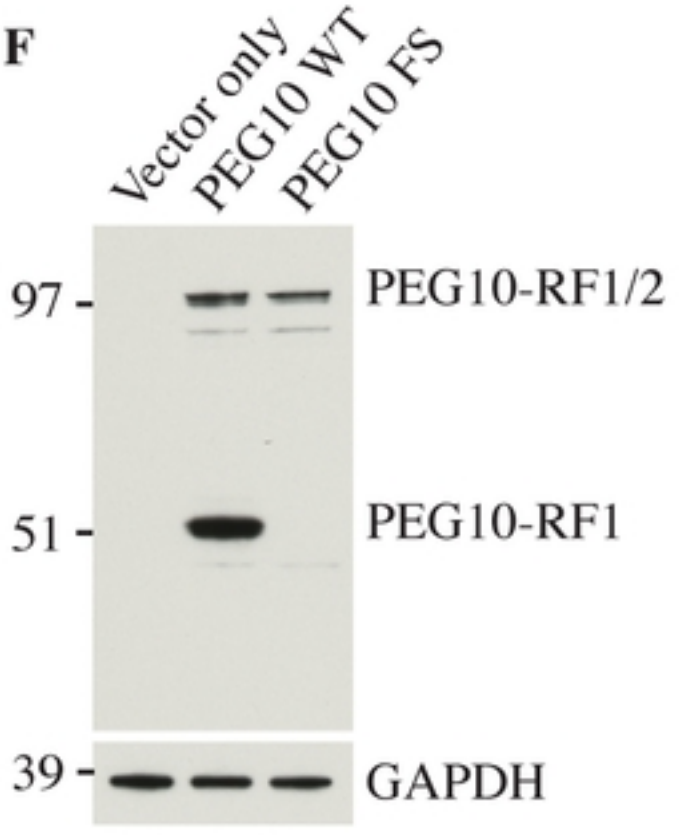

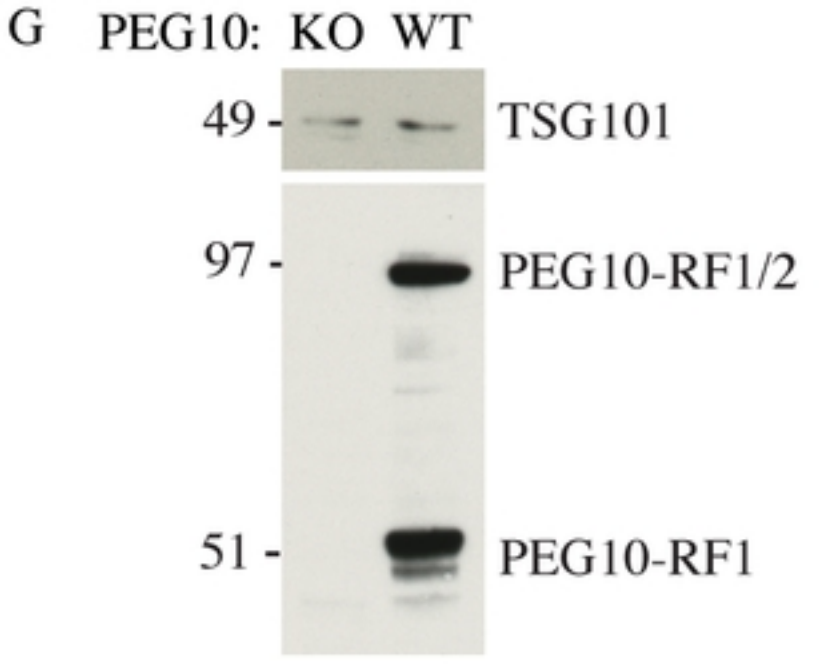

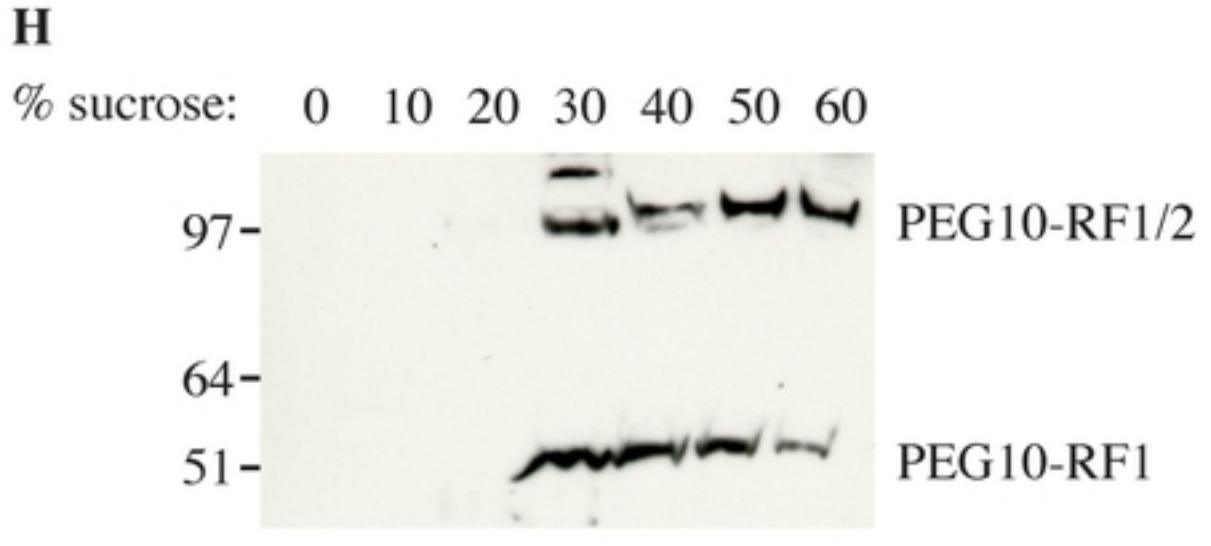

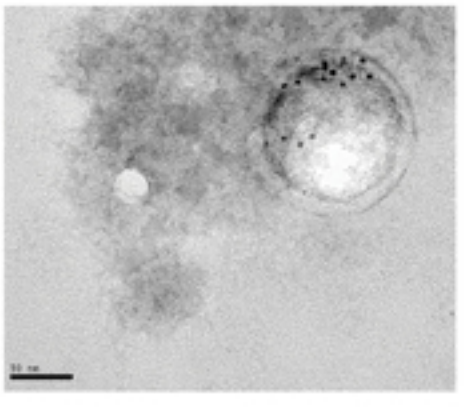

Figure 2

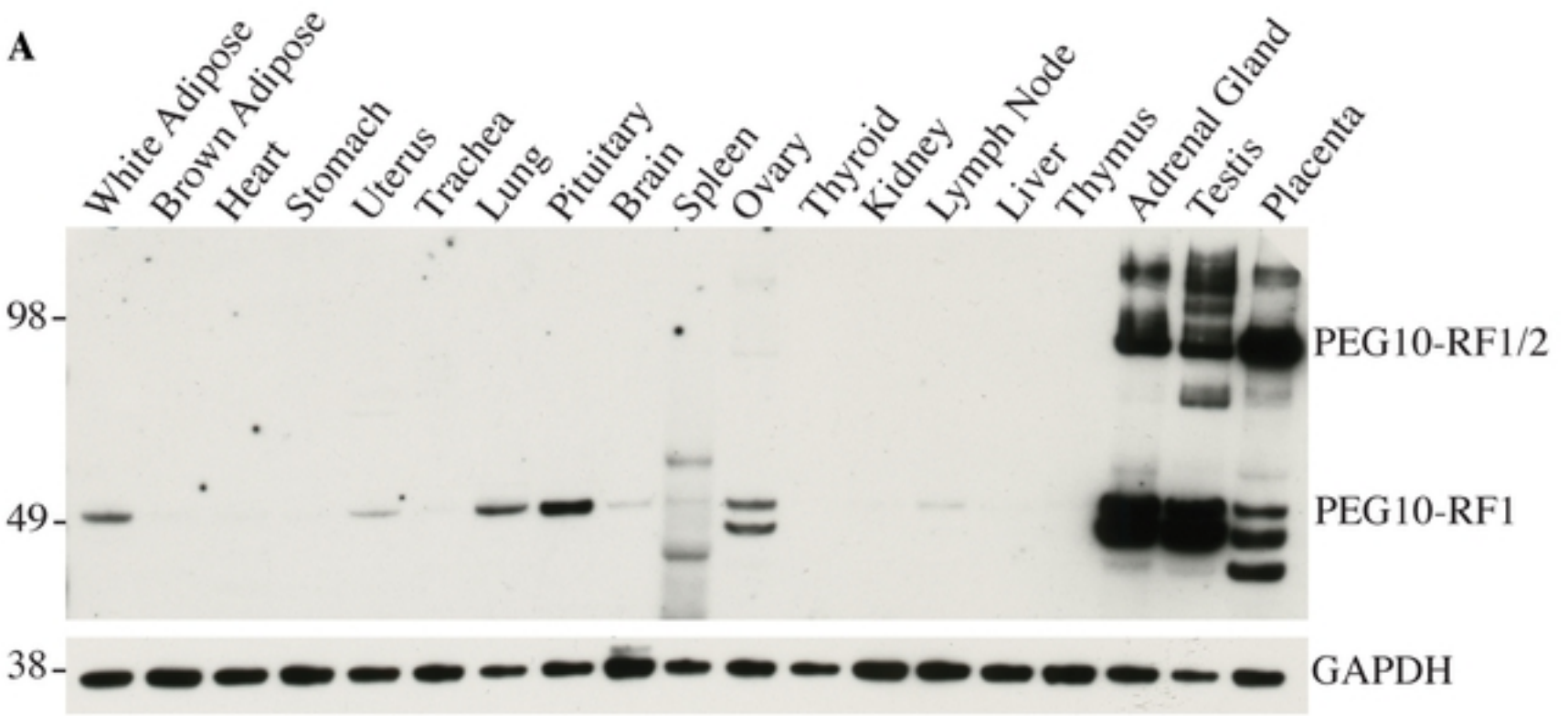

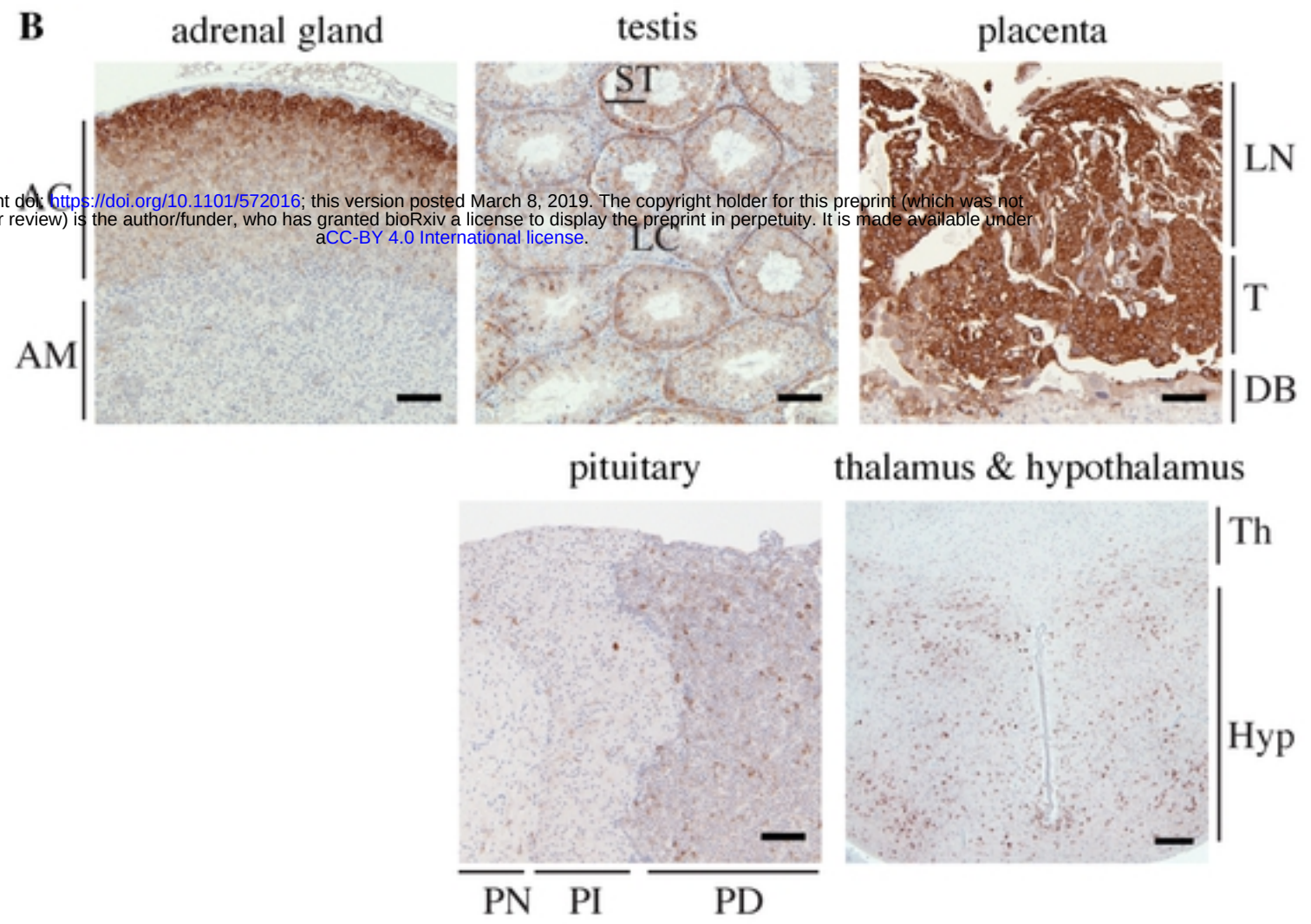

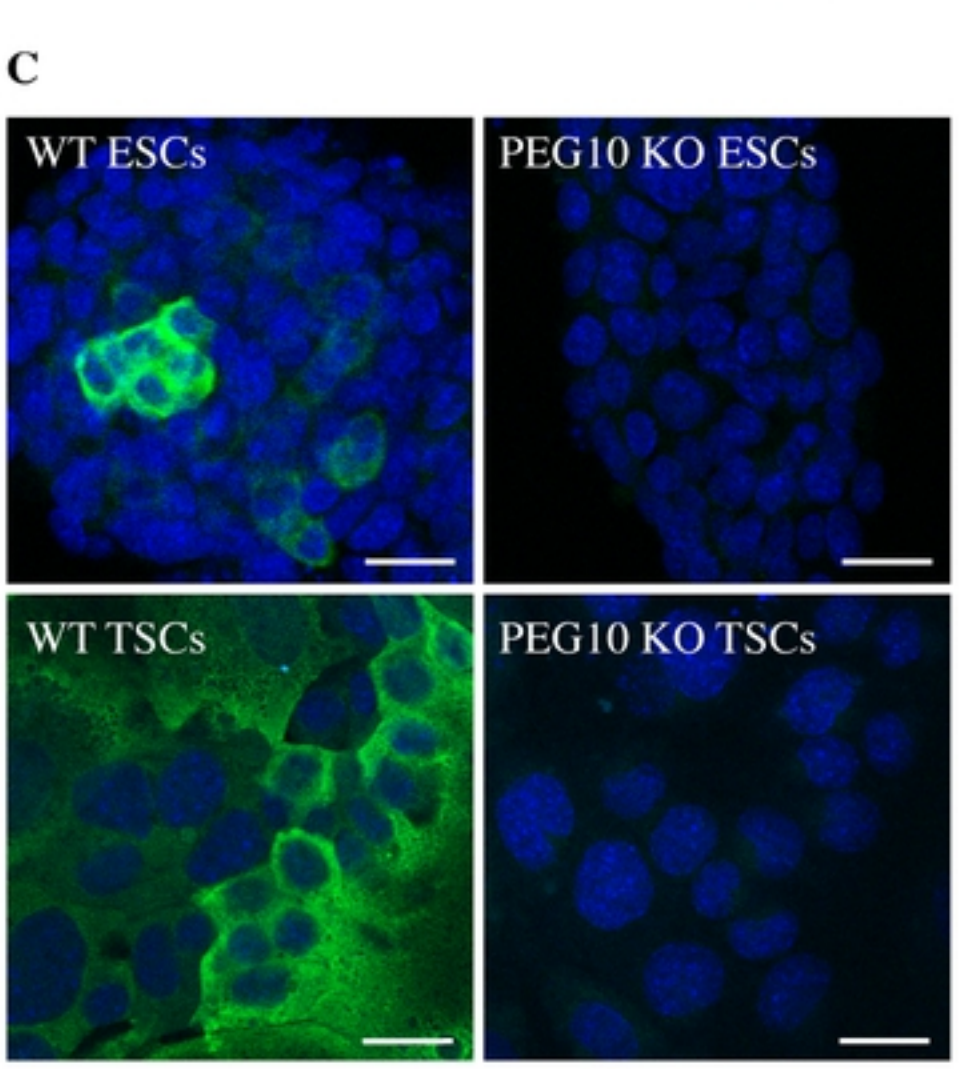

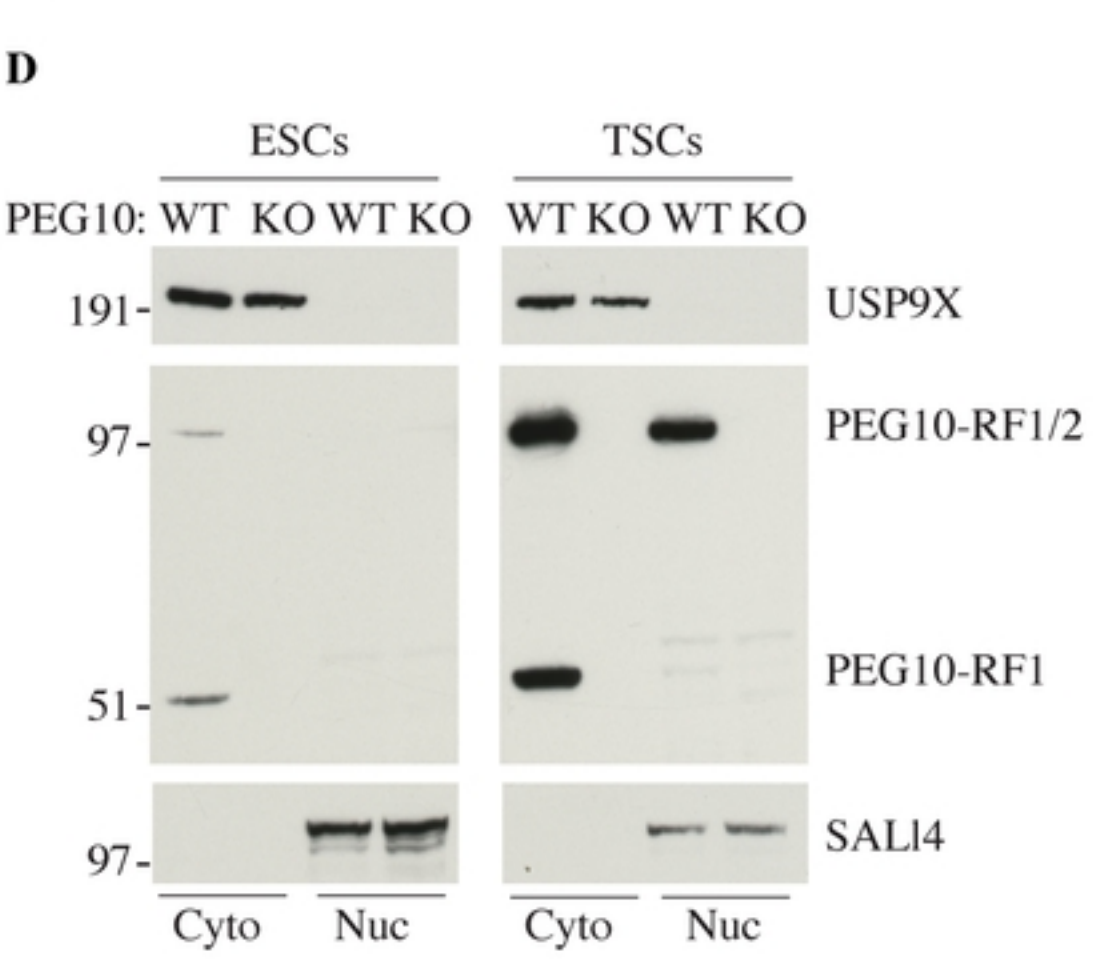

Figure 4

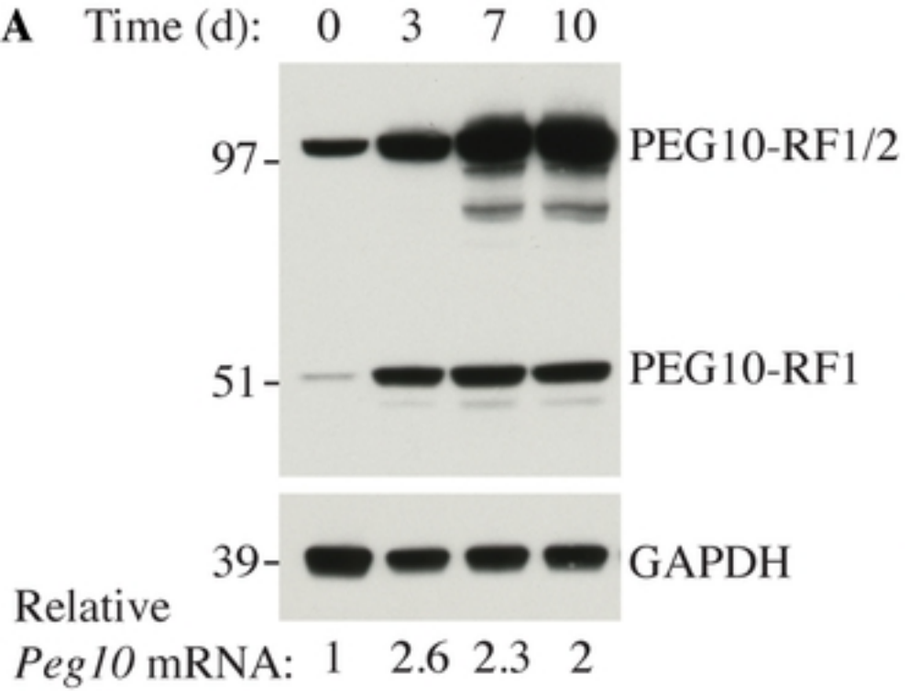
A
Time (d): 0 3 7 10
97-
PEG10-RF1/2
51-
PEG10-RF1
39-
GAPDH
Relative
Peg10 mRNA: 1 2.6 2.3 2

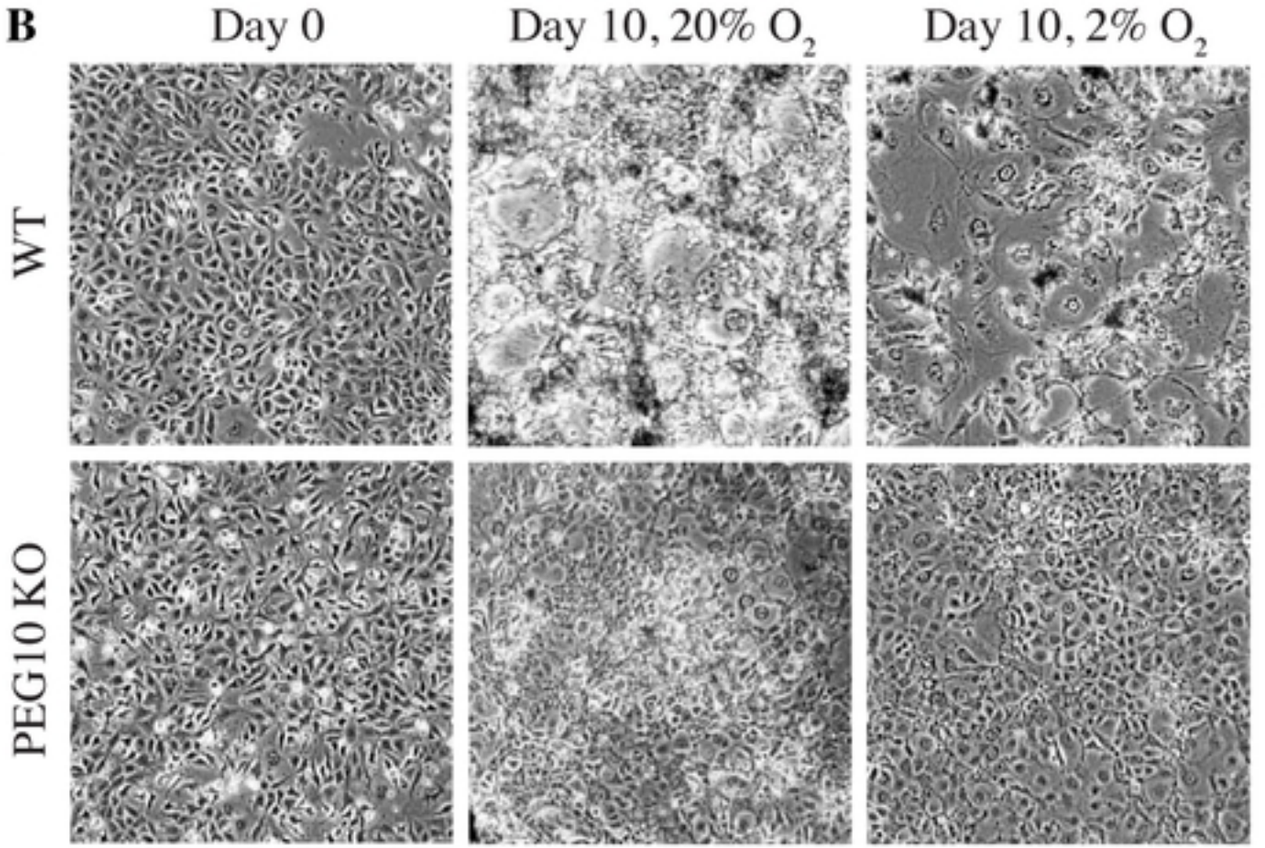
B
Day 0
Day 10, 20% O2
Day 10, 2% O2
WT
PEG10 KO

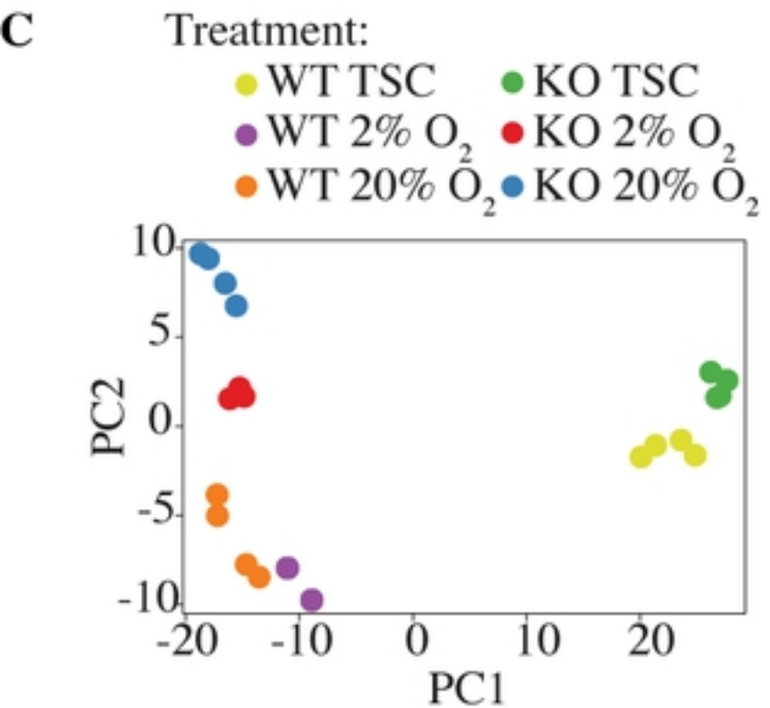
C
Treatment:
WT TSC
KO TSC
WT 2% O2
KO 2% O2
WT 20% O2
KO 20% O2
10
5
0
-5
-10
PC2
-20
-10
0
10
20
PC1

Figure 5

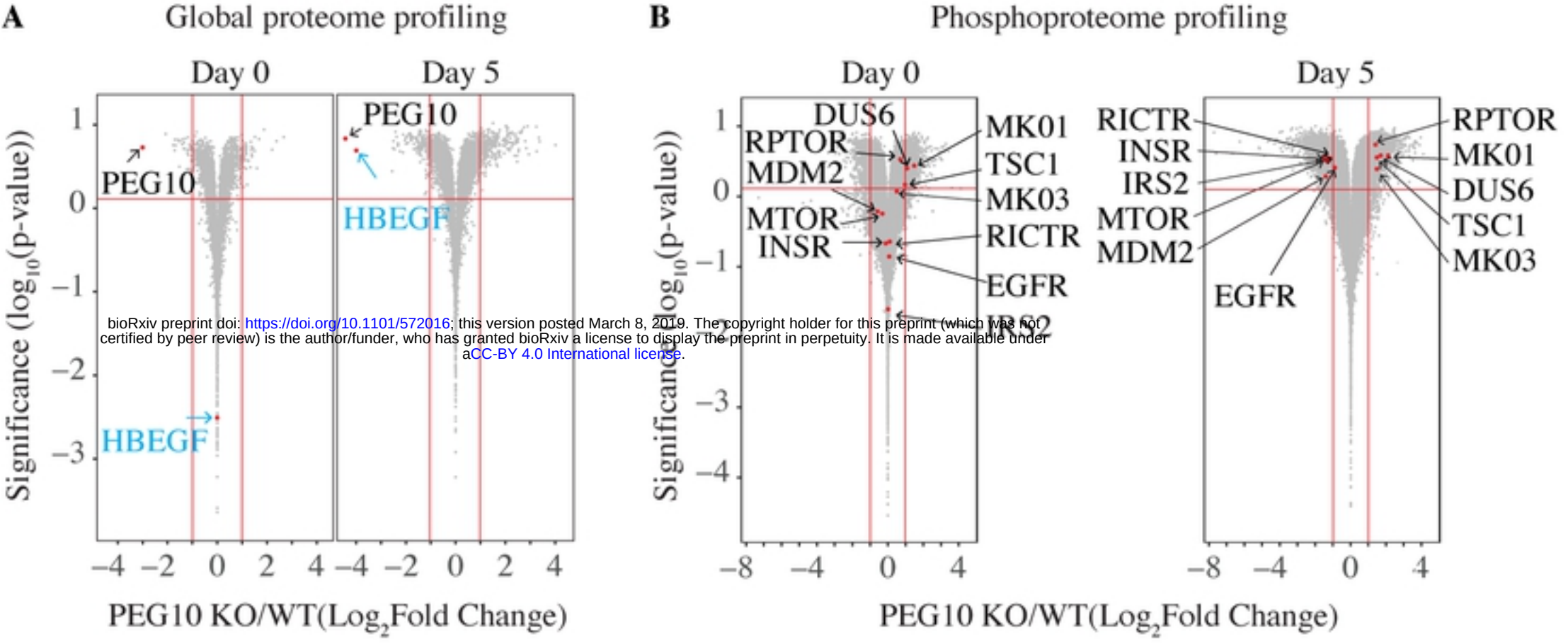

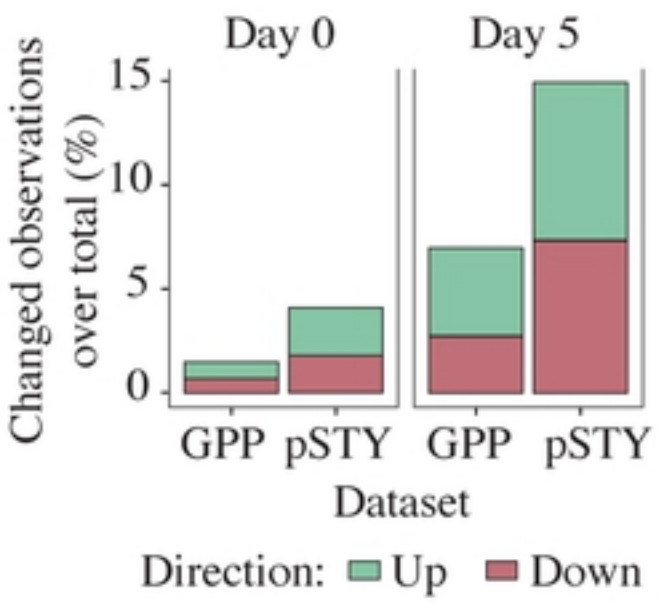

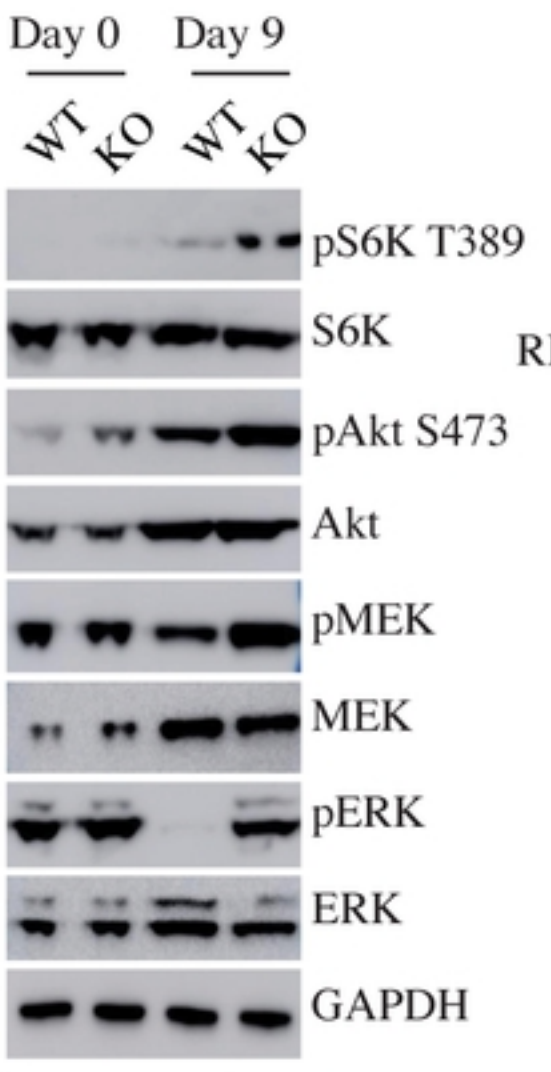

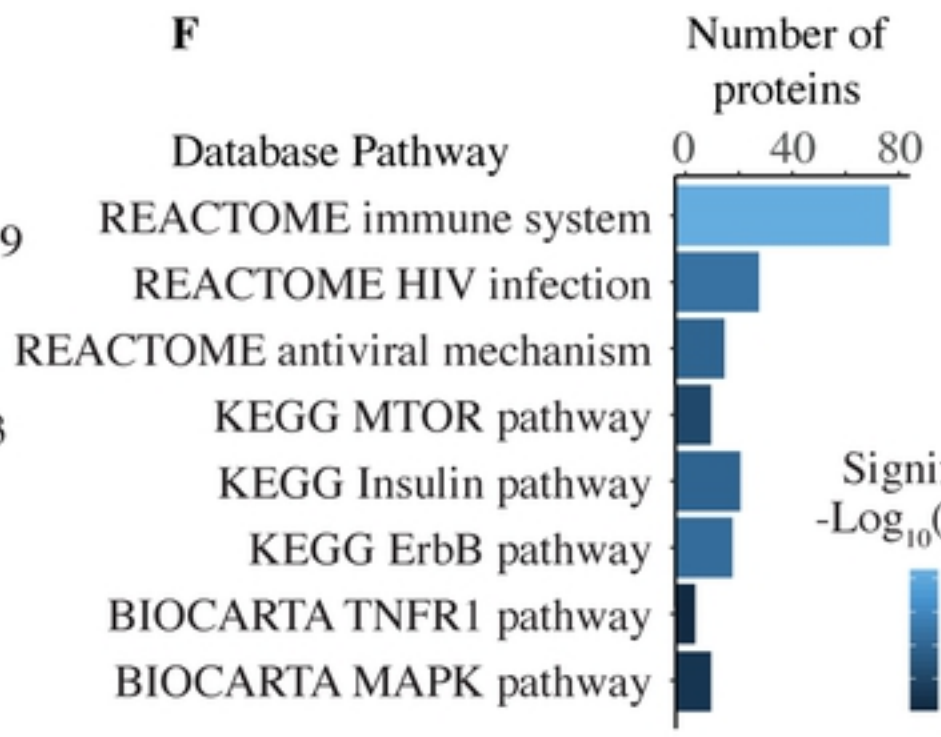

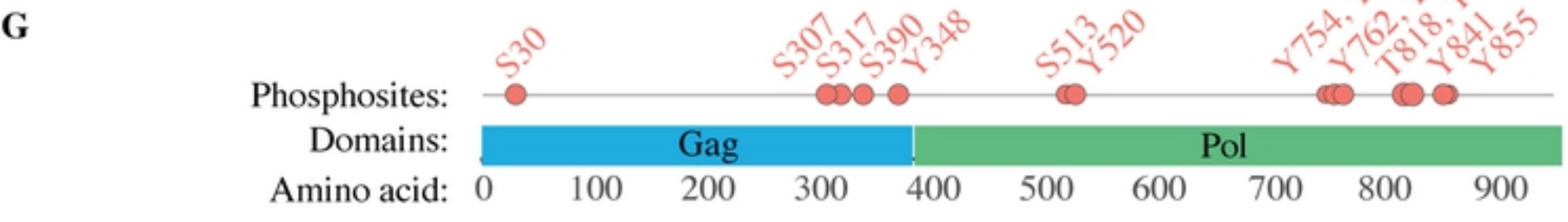

Figure 6

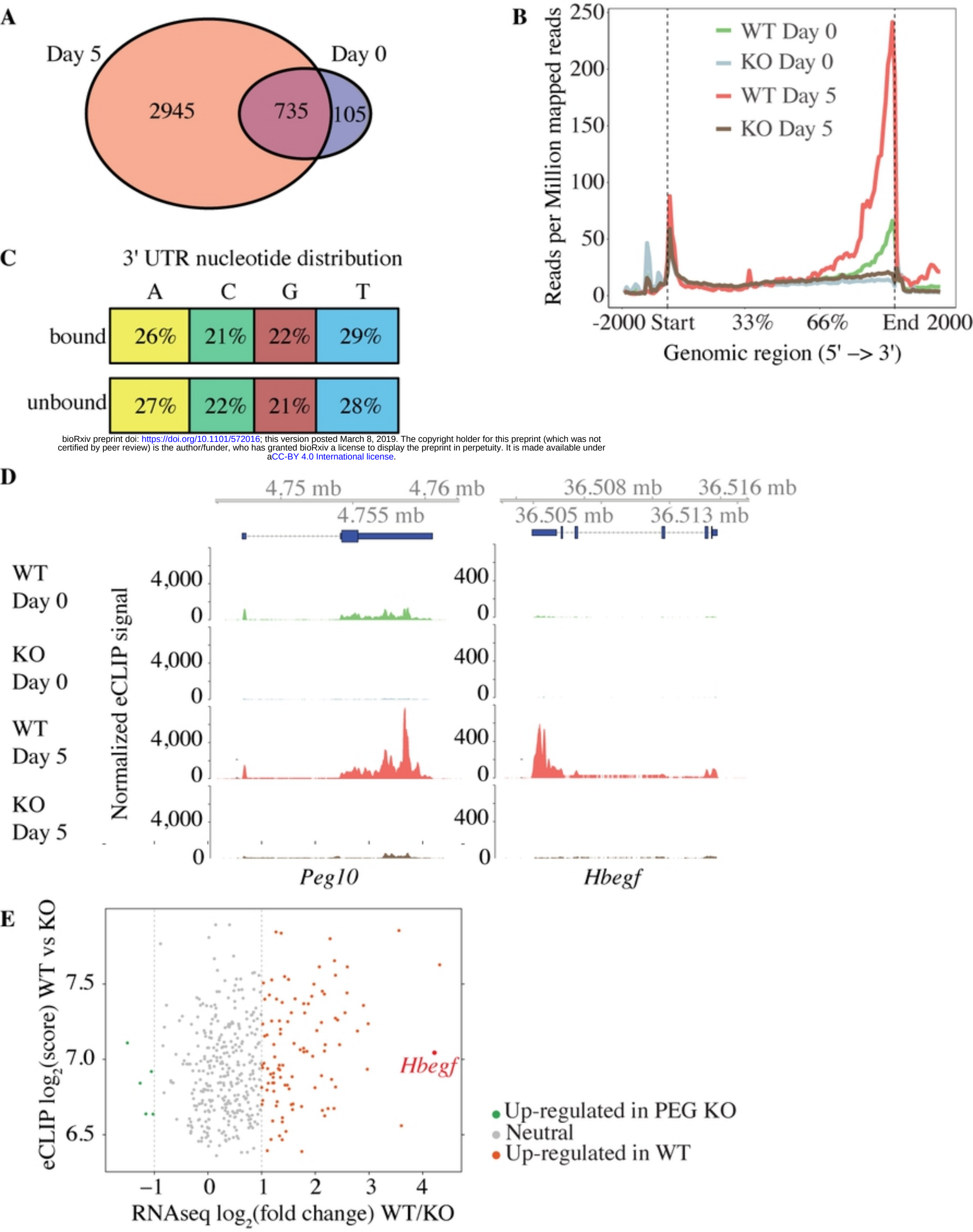

Figure 7

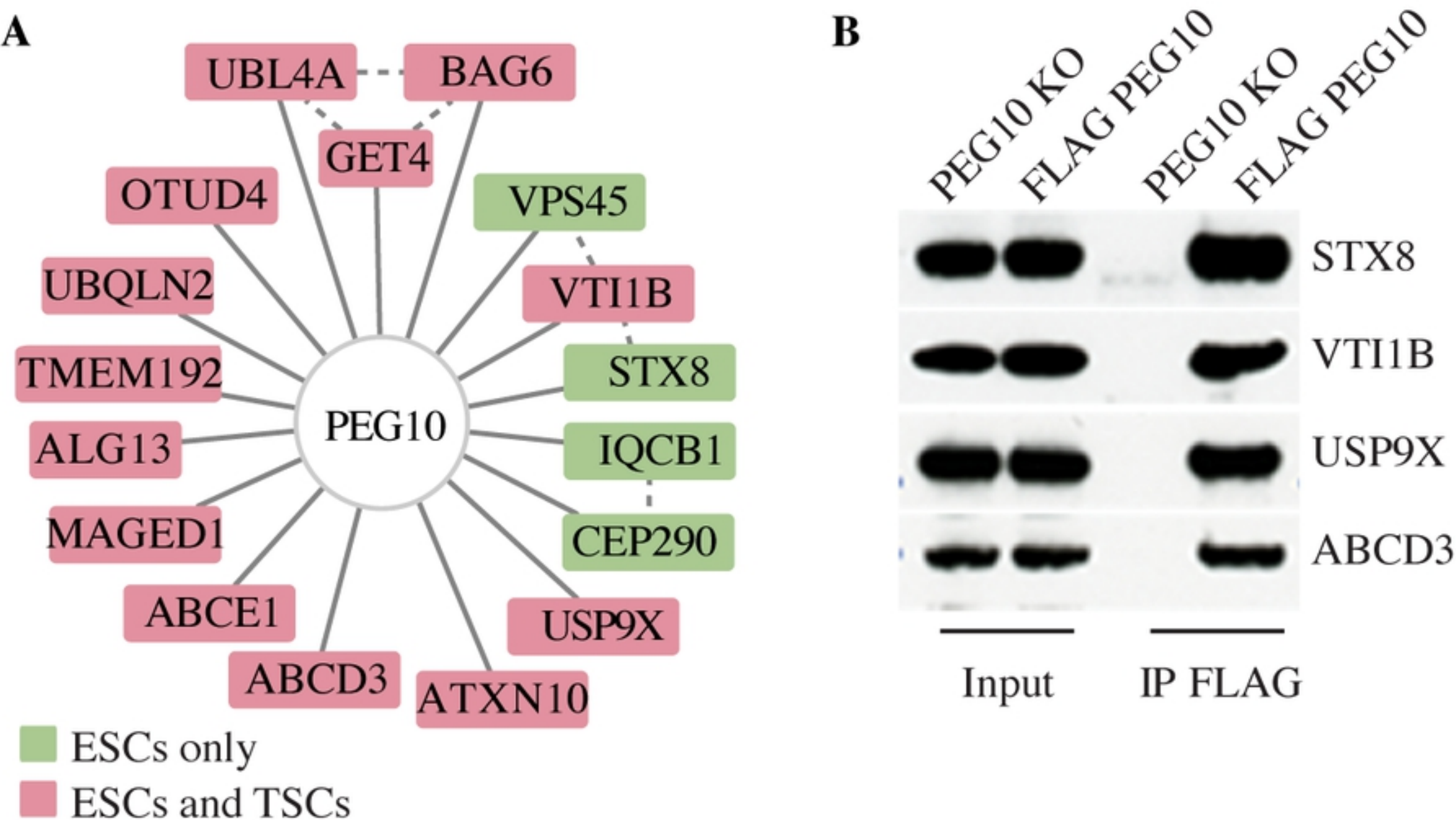
A
UBL4A
BAG6
GET4
OTUD4
VPS45
UBQLN2
VTI1B
TMEM192
STX8
PEG10
ALG13
IQCB1
MAGED1
CEP290
ABCE1
USP9X
ABCD3
ATXN10
ESCs only
ESCs and TSCs
B
PEG10 KO
FLAG PEG10
PEG10 KO
FLAG PEG10
STX8
VTI1B
USP9X
ABCD3
Input
IP FLAG

Figure 3